REPORT DOCUMENTATION PAGE Dist: A

Form Approved
OMB No. 0704-0188

1. AGENCY USE ONLY (Leave blank)	2. REPORT DATE	3. REPORT TYPE AND DATES COVERED
	18 NOV 94	Final 01 Oct 92 - 30 Sep 94

4. TITLE AND SUBTITLE
Linear Stability Analysis of Hypersonic Boundary Layers

5. FUNDING NUMBERS
F49620-92-J-0005
2307/AS

6. AUTHOR(S)
Srinivas Tadepalli, Joel Ferziger

7. PERFORMING ORGANIZATION NAME(S) AND ADDRESS(ES)
STANFORD UNIVERSITY
STANFORD, CA 94305-3030

8. PERFORMING ORGANIZATION REPORT NUMBER
AFOSR-TR- 95 0056

9. SPONSORING/MONITORING AGENCY NAME(S) AND ADDRESS(ES)
AIR FORCE OFFICE OF SCIENTIFIC RESEARCH
DIRECTORATE OF AEROSPACE SCIENCES
BOLLING AFB, DC 20332-6448
NA

10. SPONSORING/MONITORING AGENCY REPORT NUMBER
F49620-92-J-0005
2307/AS

11. SUPPLEMENTARY NOTES

12a. DISTRIBUTION/AVAILABILITY STATEMENT
APPROVED FOR PUBLIC RELEASE
DISTRIBUTION IS UNLIMITED

12b. DISTRIBUTION CODE
A

13. ABSTRACT

For linear stability analysis of high speed boundary layers, we use a direct method for its ability to yield eigenvalues without a priori knowledge and to capture all modes. Temporal linear stability analysis is performed for the 2D boundary layer on a flat plate using the local parallel flow assumption. An estimate of all the eigenvalues is obtained by solving the generalized eigenvalue problem (Malik, 1986); a local eigenvalue search is used to improve the accuracy of the most unstable eigenvalue. A compact fourth order accurate method is to compute both the mean flow and the most unstable eigenfunction. This method is more efficient than lower order methods. Local grid refinement based on error estimates is useful in providing the accuracy needed for initial conditions for direct numerical simulation of transition. Grid adaptation based on refinement yields better than power law convergence in the mean flow error.

14. SUBJECT TERMS	15. NUMBER OF PAGES
Hypersonic flow, Transition	56
	16. PRICE CODE

17. SECURITY CLASSIFICATION OF REPORT	18. SECURITY CLASSIFICATION OF THIS PAGE	19. SECURITY CLASSIFICATION OF ABSTRACT	20. LIMITATION OF ABSTRACT
UNCLASSIFIED	UNCLASSIFIED	UNCLASSIFIED	

Linear Stability Analysis of Hypersonic Boundary Layers

by
Srinivas Tadepalli
Dept. of Aeronautics & Astronautics
and
Joel H. Ferziger
Dept. of Mechanical Engineering,
Stanford University,
Stanford, California 94305-3030.

Acknowledgements: **AFOSR, SDSC**

CONTENTS

Theory and Implementation

Appendices

Linear Stability Analysis of Hypersonic Boundary Layers

by

Srinivas Tadepalli † and Joel H. Ferziger ‡

Stanford University

Stanford, California 94305.

---

1. Abstract

For linear stability analysis of high speed boundary layers, we use a direct method for its ability to yield eigenvalues without a priori knowledge and to capture all modes. Temporal linear stability analysis is performed for the 2D boundary layer on a flat plate using the local parallel flow assumption. An estimate of all the eigenvalues is obtained by solving the generalized eigenvalue problem (Malik, 1986); a local eigenvalue search is used to improve the accuracy of the most unstable eigenvalue. A compact fourth order accurate method is to compute both the mean flow and the most unstable eigenfunction. This method is more efficient than lower order methods. Local grid refinement based on error estimates is useful in providing the accuracy needed for initial conditions for direct numerical simulation of transition. Grid adaptation based on refinement yields better than power law convergence in the mean flow error.

The structure of eigenfunctions in different branches of the global spectrum is investigated. The adjoint problem is solved simultaneously at negligible computational cost and the structure of the adjoint eigenfunctions analyzed. It was observed that the normalized adjoint pressure eigenfunction is typically four orders of magnitude larger than the pressure eigenfunction, indicating that the flow is highly sensitive to mass sources.

† Graduate Student, Dept. of Aeronautics & Astronautics

‡ Professor, Dept. of Mechanical & Civil Engineering.

2. Introduction

The numerical schemes in use for solving compressible linear stability equations can be broadly classified into boundary value methods (BVM) and initial value methods (IVM). IVMs require good guesses of the eigenvalue. Although they require less memory, there is a risk of missing some modes. On the other hand, BVMs [Malik & Orszag (1981), Malik, Chuang & Hussaini (1982), Malik (1990)] require computationally intensive global searches and efficient iterative local searches. Spectral methods are not a good choice due to the movement of the critical layer from $0.2\delta \rightarrow 0.9\delta$, where δ is the boundary layer thickness, as the Mach number increases from 0 to 10. Asymptotic boundary conditions, which are analytically derived, are used in the free-stream. Spurious unstable modes are eliminated as in Malik (1982). Sutherland's law of viscosity is used for the functional dependence of viscosity on temperature. Keller's box scheme (second order) is used for comparison.

The growth or decay of infinitesimal perturbations superposed on laminar solutions of the Navier-Stokes equations is the subject of linear stability theory. In this work, the basic equations governing the linear stability of parallel-flow compressible boundary-layers are derived by linearizing the Navier-Stokes equations about the laminar flow. These perturbations are assumed to be of the form

$$u'(x,y,t) = \hat{u}(y)e^{i(\alpha x+\beta y-\omega t)}. \tag{1.1}$$

For temporal stability analysis, α, the streamwise wavenumber, is fixed and real and ω, the frequency, is complex; for spatial analysis, α is complex and ω is fixed and real. In temporal analysis, $\omega = \omega_r + i\omega_i$, ω_r is the frequency and ω_i is the growth rate of the perturbation. These infinitesimal disturbances are imposed on the compressible Navier-Stokes equations linearized about a laminar boundary layer solution. If it is assumed that the mean flow is locally parallel, a set of five ordinary differential equations is obtained. Of these, three are the second order momentum equations, one is the second order energy equation, and one is the first order continuity equation; thus the complete system is of ninth order. For reviews of boundary-layer stability theory, see Reshotko (1976), Mack (1984) or Nayfeh (1989).

LINSTAB is a compressible linear stability analysis code for two-dimensional boundary layers. It uses an iterative finite-difference method to compute the most unstable eigenvalue and requires an accurate estimate of the most-unstable eigenvalue. A local eigenvalue search procedure improves the accuracy of the eigenvalue and yields the eigenfunctions. A global procedure was developed; it may be used when no estimate of the most unstable eigenvalue is available.

The solution of the adjoint problem generally identifies regions which are important for the placement of the forcing. The adjoint eigensolution defines the efficiency with which a particular forcing excites the eigensolution.

3. Mean Flow

3.1 Governing equations

The Navier-Stokes equations governing the flow of a viscous compressible ideal gas are

$$\rho\left[\frac{\partial \boldsymbol{q}}{\partial t}+(\boldsymbol{q}.\nabla)\boldsymbol{q}\right]=\nabla.\left\{-\left(p+\frac{2}{3}\frac{\mu}{R}\nabla.\boldsymbol{q}\right)I+\frac{\mu}{R}(\nabla\boldsymbol{q}+\nabla\boldsymbol{q}^T)\right\}, \tag{3.1}$$

$$\frac{\partial \rho}{\partial t}+\nabla.(\rho\boldsymbol{q})=0, \tag{3.2}$$

$$\rho\left[\frac{\partial \theta}{\partial t}+(\boldsymbol{q}.\nabla)\theta\right]=\frac{1}{R\sigma}\nabla.(\mu\nabla\theta)+\mathrm{Ec}\left\{\frac{\partial p}{\partial t}+(\boldsymbol{q}.\nabla)p+\phi\right\}, \tag{3.3}$$

$$p=\rho\theta \tag{3.4}$$

where $\boldsymbol{q}$ is the velocity vector, ρ the density, p the pressure, θ the temperature, R the Reynolds number, Ec $(= u_e^2/(C_pT_e))$ the Eckert number, σ the Prandtl number, μ the coefficient of viscosity, and ϕ the viscous dissipation given by

$$\phi=-\frac{2}{3}\frac{\mu}{R}(\nabla.\boldsymbol{q})^2+\frac{\mu}{2R}[\nabla\boldsymbol{q}+\nabla\boldsymbol{q}^T]^2. \tag{3.5}$$

The quantities have been nondimensionalized with respect to the free-stream values. For simplicity, the Stokes approximation of zero bulk viscosity has been assumed ($\lambda/\mu = -2/3$).

The mean flow is taken to be a similarity solution of the boundary layer on a flat plate with no pressure gradient, obtained from the boundary layer approximation of the Navier-Stokes equations (3.1 - 3.5). The equations from which this solution can be derived are obtained with the aid of the Mangler-Levy-Lees transformation (White 1991, p. 534) for two-dimensional flow

$$d\xi = \rho_e \mu_e u_e dx, \tag{3.6}$$

$$d\eta = \left[\rho u_e/(2\xi)^{1/2}\right] dy. \tag{3.7}$$

If constant properties are assumed, Eqs. (3.1 - 3.4) reduce to

$$(cf'')' + ff'' = 0 \tag{3.8}$$

$$(a_1 g' + a_2 f' f'')' + fg' = 0 \tag{3.9}$$

where a prime denotes differentiation with respect to η.

The boundary conditions become

$$f(0) = f_w, \qquad f'(0) = 0, \qquad \lim_{\eta\to\infty} f'(\eta) = 1, \tag{3.10}$$

$$g(0) = g_w, \qquad \lim_{\eta\to\infty} g(\eta) = 1. \tag{3.11}$$

In these equations:

$$f' \equiv u/u_e, \qquad c \equiv \rho\mu/\rho_e\mu_e,$$

$$g \equiv H/H_e, \qquad a_1 \equiv c/\sigma, \qquad a_2 \equiv \frac{(\gamma-1)M^2}{1+\left(\frac{\gamma-1}{2}\right)M^2}\left(1-\frac{1}{\sigma}\right)c$$

and H is the enthalpy, γ the ratio of specific heats, u_e, ρ_e, μ_e, H_e the edge values of the velocity, density, viscosity and enthalpy, and M the edge Mach number defined as $M = \frac{u_e}{\sqrt{\gamma \Re T_e}}$. The Prandtl number σ is defined as $\sigma = \frac{\mu c_p}{k}$, where c_p is the

specific heat at constant pressure and is assumed to be constant. The viscosity μ is assumed to be given by the Sutherland formula

$$\mu = 1.46 \times 10^{-6} \frac{T^{1/2}}{1 + 110.3/T} \quad N.sm^{-2}.$$

The thermal conductivity k is computed using $\sigma = 0.7$. Atlternatively, the profiles could be provided numerically by the user. For example, they could be obtained from a two–dimensional boundary layer calculation.

Compressible Linear Stability Equations

Now we describe the procedures for temporal stability analysis. The procedures for spatial analysis are the same but the roles of ω and α are exchanged. Following Eqs. (3.1)-(3.5), let $\boldsymbol{Q}$, P, T and ρ_m be the velocity, pressure, temperature and density of the steady mean flow, and $\boldsymbol{q}'$, p', T', and ρ' the velocity, pressure, temperature and density of the disturbance. Then $\boldsymbol{q} = \boldsymbol{Q} + \boldsymbol{q}'$, $p = P + p'$, $\theta = T + T'$, $\rho = \rho_m + \rho'$ and $\boldsymbol{Q}$, P, T, ρ_m satisfy the Eqs. (3.1)-(3.5). Subtracting the equations for the mean flow from the full equations, linearizing around the mean flow, assuming the mean flow to be locally parallel ($\boldsymbol{Q} = (U(y), 0, W(y))$, no pressure gradient across the boundary layer ($p = 1$ and $\rho_m = 1/T$), and the disturbance to have the form

$$\begin{aligned}
\boldsymbol{q}' &= \begin{pmatrix} u' \\ v' \\ w' \end{pmatrix} = \begin{pmatrix} \tilde{u}(y) \\ \tilde{v}(y) \\ \tilde{w}(y) \end{pmatrix} \exp\left[\mathrm{i}(\alpha x + \beta z - \omega t)\right], \\
p' &= \tilde{p}(y) \exp\left[\mathrm{i}(\alpha x + \beta z - \omega t)\right] \\
T' &= \tilde{T}(y) \exp\left[\mathrm{i}(\alpha x + \beta z - \omega t)\right]. \qquad (3.12)
\end{aligned}$$

to obtain the following equations,

$$\left[\mathrm{i}\frac{1}{T}(\alpha U+\beta W-\omega)+\frac{\mu}{R}(l_2\alpha^2+\beta^2)\right]\tilde{u}+\left(\frac{1}{T}\frac{\partial U}{\partial y}-\frac{\mathrm{i}}{R}\frac{\partial \mu}{\partial y}\alpha\right)\tilde{v}+\mathrm{i}\alpha\tilde{p}$$
$$+\frac{l_1}{R}\mu\alpha\beta\tilde{w}-\frac{1}{R}\left\{\frac{\partial}{\partial y}\left(\mu'\frac{\partial U}{\partial y}\right)\tilde{T}+\frac{\partial U}{\partial y}\frac{\partial \tilde{u}}{\partial y}\right.$$
$$\left.+\mathrm{i}l_1\mu\alpha\frac{\partial \tilde{v}}{\partial y}+\mu'\frac{\partial U}{\partial y}\frac{\partial \tilde{T}}{\partial y}+\mu\frac{\partial^2\tilde{u}}{\partial y^2}\right\}=0. \tag{3.13}$$

$$\left[\mathrm{i}\frac{1}{T}(\alpha U+\beta W-\omega)+\frac{\mu}{R}(\alpha^2+\beta^2)\right]\tilde{v}+\frac{\partial \tilde{p}}{\partial y}$$
$$-\frac{1}{R}\left\{\mathrm{i}l_0\frac{\partial \mu}{\partial y}[\alpha\tilde{u}+\beta\tilde{w}]+\mathrm{i}\mu'\left(\alpha\frac{\partial U}{\partial y}+\beta\frac{\partial W}{\partial y}\right)\tilde{T}\right.$$
$$\left.+\mathrm{i}l_1\mu\left(\alpha\frac{\partial \tilde{u}}{\partial y}+\beta\frac{\partial \tilde{w}}{\partial y}\right)+l_2\frac{\partial \mu}{\partial y}\frac{\partial \tilde{v}}{\partial y}+l_2\mu\frac{\partial^2\tilde{v}}{2}\right\}=0, \tag{3.14}$$

$$\left[\mathrm{i}\frac{1}{T}(\alpha U+\beta W-\omega)+\frac{\mu}{R}(\alpha^2+l_2\beta^2)\right]\tilde{w}+\left(\frac{1}{T}\frac{\partial W}{\partial y}-\frac{\mathrm{i}}{R}\frac{\partial \mu}{\partial y}\beta\right)\tilde{v}+\mathrm{i}\beta\tilde{p}$$
$$+\frac{l_1}{R}\mu\alpha\beta\tilde{u}-\frac{1}{R}\left\{\frac{\partial}{\partial y}\left(\mu'\frac{\partial W}{\partial y}\right)\tilde{T}+\frac{\partial W}{\partial y}\frac{\partial \tilde{w}}{\partial y}\right.$$
$$\left.+\mathrm{i}l_1\mu\beta\frac{\partial \tilde{v}}{\partial y}+\mu'\frac{\partial W}{\partial y}\frac{\partial \tilde{T}}{\partial y}+\mu\frac{\partial^2\tilde{w}}{\partial y^2}\right\}=0. \tag{3.15}$$

$$\mathrm{i}\frac{1}{T}(\alpha\tilde{u}+\beta\tilde{w})+\mathrm{i}(\alpha U+\beta W-\omega)\tilde{\rho}+\frac{\partial}{\partial y}(\frac{1}{T}\tilde{v})=0, \tag{3.16}$$

$$\left[\mathrm{i}\frac{1}{T}(\alpha U+\beta W-\omega)-\frac{(\gamma-1)M^2}{R}\mu'\left\{\left(\frac{\partial U}{\partial y}\right)^2+\left(\frac{\partial W}{\partial y}\right)^2\right\}\right.$$
$$\left.+\frac{1}{R\sigma}\left\{\mu(\alpha^2+\beta^2)-\frac{\partial^2\mu}{\partial y^2}\right\}\right]\tilde{T}$$
$$+\left[\frac{1}{T}\frac{\partial T}{\partial y}-\frac{2\mathrm{i}(\gamma-1)M^2}{R}\mu\left(\alpha\frac{\partial U}{\partial y}+\beta\frac{\partial W}{\partial y}\right)\right]\tilde{v}$$
$$-\mathrm{i}(\gamma-1)M^2(\alpha U+\beta W-\omega)\tilde{p}$$
$$-\frac{2(\gamma-1)M^2}{R}\mu\left(\frac{\partial U}{\partial y}\frac{\partial \tilde{u}}{\partial y}+\frac{\partial W}{\partial y}\frac{\partial \tilde{w}}{\partial y}\right)-\frac{1}{R\sigma}\left[2\frac{\partial \mu}{\partial y}\frac{\partial \tilde{T}}{\partial y}+\mu\frac{\partial^2\tilde{T}}{\partial y^2}\right]=0. \tag{3.17}$$

where γ is the ratio of the specific heats, σ the Prandtl number, R the Reynolds number based on the displacement thickness δ^*, M the Mach number, and $l_j = j + \lambda/\mu$.

With the above asumptions, the equation of state (3.4) simplifies to

$$\tilde{\rho} = \gamma M^2 \frac{\tilde{p}}{T} - \frac{\tilde{T}}{T^2} \tag{3.18}$$

which was used to eliminate density $\tilde{\rho}$ from (3.13)-(3.17).

The boundary conditions are

$$\tilde{u} = \tilde{v} = \tilde{w} = \tilde{T} = 0 \quad \text{at} \quad y = 0, \tag{3.19}$$

$$\tilde{u}, \tilde{v}, \tilde{w}, \tilde{T} \to 0 \quad \text{as} \quad y \to \infty. \tag{3.20}$$

They are the linear stability equations for the compressible parallel flow.

3.2 Numerical solution schemes

To solve Eqs. (3.8)-(3.9), Keller's Box Method is used. This method is described in great detail by Cebecci and Smith (1974). We will apply it to the two-dimensional flow.

We first write Eqs. (3.8) and (3.9) as a first-order system of ordinary differential equations. For that purpose, we introduce new dependent variables $u(\eta)$ and $v(\eta)$ so that the momentum equation (3.8) can be written

$$f' = u \tag{3.21a}$$

$$u' = v \tag{3.21b}$$

$$(cv)' + fv = 0 \tag{3.21c}$$

In terms of these variables, the boundary conditions become

$$f(0) = f_w, \qquad u(0) = 0, \qquad \lim_{\eta \to \infty} u(\eta) = 1, \tag{3.22}$$

and, introducing a new function $G(\eta)$, the energy equation (3.9) can be written

$$(a_1 G)' + fG + (a_2 uv)' = 0 \tag{3.23a}$$

$$g' = G \tag{3.23b}$$

along with boundary conditions

$$g(0) = g_w \quad or \quad G(0) = G_w, \qquad \lim_{\eta \to \infty} g(\eta) = 1, \tag{3.24}$$

3.2.1 Second-order difference scheme

The discretization is based on Keller's Box Method.

Momentum equation

We denote (f, u, v) at (η_j) by (f_j, u_j, v_j). The discretized form of Eqs. (3.21) is obtained by integrating each equation from η_{j-1} to η_j and using the trapezoid rule to approximate any integral:

$$f_j - f_{j-1} - \tfrac{1}{2} h_j (u_j + u_{j-1}) = 0, \tag{3.25a}$$

$$(cv)_j - (cv)_{j-1} + \tfrac{1}{2} h_j \left((fv)_j + (fv)_{j-1} \right) = 0, \tag{3.25b}$$

$$u_{j+1} - u_j - \tfrac{1}{2} h_{j+1} (v_{j+1} + v_j) = 0, \tag{3.25c}$$

The boundary conditions are

$$f_1 = f_w, \qquad u_1 = 0, \qquad u_J = 1, \tag{3.26}$$

and $h_j = \eta_j - \eta_{j-1}$.

A Newton iteration method is used to solve the non-linear system (3.25) along with boundary conditions (3.26). If the superscript i denotes the value of the variable at the ith Newton iteration, then

$$f_j^{(i+1)} = f_j^{(i)} + \delta f_j^{(i)}$$
$$u_j^{(i+1)} = u_j^{(i)} + \delta u_j^{(i)}$$
$$v_j^{(i+1)} = v_j^{(i)} + \delta v_j^{(i)}.$$

Linearizing the system (3.25) about the solution at iteration i by dropping the terms quadratic in δ-quantities, we obtain the linear system

$$\delta f_j - \delta f_{j-1} - \tfrac{1}{2}h_j(\delta u_j + \delta u_{j-1}) = r_j, \tag{3.27a}$$

$$c_j \delta v_j - c_{j-1}\delta v_{j-1} = s_j, \tag{3.27b}$$

$$\delta u_{j+1} - \delta u_j - \tfrac{1}{2}h_{j+1}(\delta v_{j+1} + \delta v_j) = t_j, \tag{3.27c}$$

where

$$\begin{aligned} r_j &= -\left(f_j - f_{j-1} - \tfrac{1}{2}h_j(u_j + u_{j-1})\right) \\ s_j &= -\left(c_j v_j - c_{j-1}v_{j-1} + \tfrac{1}{2}h_j\left(f_j v_j + f_{j-1}v_{j-1}\right)\right) \\ t_j &= -\left(u_{j+1} - u_j - \tfrac{1}{2}h_{j+1}(v_{j+1} + v_j)\right) \end{aligned}$$

The system (3.27) is linear and has block tridiagonal structure and so may be written as

$$C_j \underline{\delta}_{j+1} + A_j \underline{\delta}_j + B_j \underline{\delta}_{j-1} = \underline{r}_j,$$

where

$$\underline{\delta}_j = \begin{bmatrix} \delta f_j \\ \delta u_j \\ \delta v_j \end{bmatrix}, \qquad \underline{r}_j = \begin{bmatrix} r_j \\ s_j \\ t_j \end{bmatrix},$$

and, for $j = 2, 3, ..., J-1$,

$$C_j = \begin{bmatrix} 0 & 0 & 0 \\ 0 & 0 & 0 \\ 0 & 1 & -\frac{1}{2}h_{j+1} \end{bmatrix}$$

$$A_j = \begin{bmatrix} 1 & -\frac{1}{2}h_j & 0 \\ 0 & 0 & \frac{c_j}{h_j} \\ 0 & -1 & -\frac{1}{2}h_{j+1} \end{bmatrix}$$

$$B_j = \begin{bmatrix} -1 & -\frac{1}{2}h_j & 0 \\ 0 & 0 & -\frac{c_{j-1}}{h_j} \\ 0 & 0 & 0 \end{bmatrix}$$

The boundary conditions are

$$\delta f_1 = 0, \qquad \delta u_1 = 0 \qquad \textit{and} \quad \delta u_J = 0$$

so that, at the wall,

$$A_1 = \begin{bmatrix} 1 & 0 & 0 \\ 0 & 1 & 0 \\ 0 & -1 & -\frac{1}{2}h_2 \end{bmatrix}, \quad C_1 = \begin{bmatrix} 0 & 0 & 0 \\ 0 & 0 & 0 \\ 0 & 1 & -\frac{1}{2}h_2 \end{bmatrix}, \quad \underline{r}_1 = \begin{bmatrix} 0 \\ 0 \\ t_1 \end{bmatrix}$$

and, at the free-stream,

$$A_J = \begin{bmatrix} 1 & -\frac{1}{2}h_J & 0 \\ 0 & 0 & \frac{c_J}{h_J} \\ 0 & 1 & 0 \end{bmatrix}, \quad B_J = \begin{bmatrix} -1 & -\frac{1}{2}h_J & 0 \\ 0 & 0 & -\frac{c_{J-1}}{h_J} \\ 0 & 0 & 0 \end{bmatrix}, \quad \underline{r}_J = \begin{bmatrix} r_J \\ s_J \\ 0 \end{bmatrix}.$$

This system is solved by means of block-tridiagonal factorization as described in Cebeci and Smith (1974, §7). The quantities (f_j, u_j, v_j) are updated with $(\delta f_j, \delta u_j, \delta v_j)$ and the process is repeated until convergence within preassigned tolerance (10^{-10}) is achieved.

Energy equation

The energy equation is coupled to the momentum equation through the fluid properties like viscosity and thermal conductivity. However, once these parameters and f, u and v are known, the energy equation becomes linear.

We assume initial enthalpy and velocity profiles and compute the fluid properties and then solve momentum equations followed by the energy equation iterating until the convergence criterion is met.

Eqs. (3.23) are linear and their discretized form is

$$\frac{(a_1 G)_j - (a_1 G)_{j-1}}{h_j} + \tfrac{1}{2}(f_j G_j + f_{j-1} G_{j-1}) = t_j, \qquad (3.28a)$$

$$g_{j+1} - g_j - \tfrac{1}{2}h_{j+1}(G_{j+1} + G_j) = 0, \qquad (3.28b)$$

along with boundary conditions

$$G_1 = G_w = 0 \qquad \textit{and} \qquad g_J = 1.$$

As for the momentum equations, Eqs. (3.28) are written in a block-tridiagonal form

$$C_j \underline{\delta}_{j+1} + A_j \underline{\delta}_j + B_j \underline{\delta}_{j-1} = \underline{r}_j,$$

where

$$\underline{\delta}_j = \begin{bmatrix} g_j \\ G_j \end{bmatrix}, \qquad \underline{r}_j = \begin{bmatrix} t_j \\ 0 \end{bmatrix},$$

with

$$t_j = -\frac{1}{h_j}\left((a_2 uv)_j + (a_2 uv)_{j-1}\right),$$

and, for $j = 2, 3, ..., J-1$,

$$C_j = \begin{bmatrix} 0 & 0 \\ 1 & -\frac{1}{2}h_{j+1} \end{bmatrix}$$
$$A_j = \begin{bmatrix} 0 & \frac{(a_1)_j}{h_j} + \frac{1}{2}f_j \\ -1 & -\frac{1}{2}h_{j+1} \end{bmatrix}$$
$$B_j = \begin{bmatrix} 0 & -\frac{(a_1)_{j-1}}{h_j} + \frac{1}{2}f_{j-1} \\ 0 & 0 \end{bmatrix}.$$

The boundary conditions give rise to special cases: At the wall,

$$A_1 = \begin{bmatrix} 0 & 1 \\ -1 & -\frac{1}{2}h_2 \end{bmatrix}, \quad C_1 = \begin{bmatrix} 0 & 0 \\ 1 & -\frac{1}{2}h_2 \end{bmatrix}, \quad \underline{r}_1 = \begin{bmatrix} 0 \\ 0 \end{bmatrix}$$

wile, at the free stream,

$$A_J = \begin{bmatrix} 0 & \frac{(a_1)_J}{h_J} + \frac{1}{2}f_J \\ 1 & 0 \end{bmatrix}, \quad B_J = \begin{bmatrix} 0 & -\frac{(a_1)_{J-1}}{h_J} + \frac{1}{2}f_{J-1} \\ 0 & 0 \end{bmatrix}, \quad \underline{r}_J = \begin{bmatrix} t_J \\ 1 \end{bmatrix}.$$

This system is solved by means of block-tridiagonal factorization.

3.2.2 Fourth-order compact difference scheme

A fourth-order accurate two-point scheme can be derived by means of the Euler-Maclaurin formula

$$\Psi^k - \Psi^{k-1} = \frac{h_k}{2}\left(\frac{d\Psi^k}{dy} + \frac{d\Psi^{k-1}}{dy}\right) - \frac{h_k^2}{12}\left(\frac{d^2\Psi^k}{dy^2} - \frac{d^2\Psi^{k-1}}{dy^2}\right) + O(h_k^5), \quad (3.29)$$

where $\Psi^k = \Psi(y_k)$ and $h_k = y_k - y_{k-1}$.

This high-order numerical method was first used for boundary layers by Wornom (1977) who demonstrated its efficiency compared to other fourth-order methods, especially when non-regular meshes are used. Iyer and Harris (1989, 1990) present computations using this compact scheme for three-dimensional compressible boundary layers.

The strong point of this scheme is that only two data points are required and grid smoothness is not crucial for high accuracy. Second order local computations are sensitive to stretching functions.

Momentum equation

We apply formula (3.29) to Eqs. (3.21) with

$$\Psi^k = \begin{bmatrix} f_k \\ v_k \\ u_k \end{bmatrix}$$

so that

$$\frac{d\Psi^k}{dy} = A_k \Psi^k \qquad and \qquad \frac{d^2\Psi^k}{dy^2} = B_k \Psi^k$$

where

$$A_k = \begin{bmatrix} 0 & 0 & 1 \\ -\frac{v_k}{c_k} & -\frac{c'_k}{c_k} & 0 \\ 0 & 1 & 0 \end{bmatrix}, \qquad B_k = \begin{bmatrix} 0 & 1 & 0 \\ \frac{f_k v_k}{c_k^2} + \frac{3 v_k c'_k}{c_k^2} & -\frac{c''_k}{c_k} + 2\left(\frac{c'_k}{c_k}\right)^2 & -\frac{v_k}{c_k} \\ -\frac{v_k}{c_k} & -\frac{c'_k}{c_k} & 0 \end{bmatrix}.$$

$$A_k^+ = \begin{bmatrix} 0 & 0 & 1 \\ -\frac{v_k}{c_k} & -\frac{c'_k}{c_k} & 0 \\ 0 & 0 & 0 \end{bmatrix}, \qquad A_k^- = \begin{bmatrix} 0 & 0 & 0 \\ 0 & 0 & 0 \\ 0 & 1 & 0 \end{bmatrix};$$

$$B_k^+ = \begin{bmatrix} 0 & 1 & 0 \\ \frac{f_k v_k}{c_k^2} + \frac{3 v_k c'_k}{c_k^2} & -\frac{c''_k}{c_k} + 2\left(\frac{c'_k}{c_k}\right)^2 & -\frac{v_k}{c_k} \\ 0 & 0 & 0 \end{bmatrix}, \qquad B_k^- = \begin{bmatrix} 0 & 0 & 0 \\ 0 & 0 & 0 \\ -\frac{v_k}{c_k} & -\frac{c'_k}{c_k} & 0 \end{bmatrix};$$

so that

$$\begin{bmatrix} f_k - f_{k-1} \\ v_k - v_{k-1} \\ u_k - u_{k+1} \end{bmatrix} = \frac{h_k}{2}\left(A_k^+\Psi^k + A_{k-1}^+\Psi^{k-1}\right) - \frac{h_k^2}{12}\left(B_k^+\Psi^k - B_{k-1}^+\Psi^{k-1}\right)$$

$$-\frac{h_{k+1}}{2}\left(A_{k+1}^-\Psi^{k+1} + A_k^-\Psi^k\right) + \frac{h_{k+1}^2}{12}\left(B_{k+1}^-\Psi^{k+1} - B_k^-\Psi^k\right). \qquad (3.30)$$

These equations can be written in the block-tridiagonal form

$$R_k\Psi^{k+1} + P_k\Psi^k + Q_k\Psi^{k-1} = 0 \qquad (3.31)$$

where

$$P_k = I - \frac{h_k}{2}A_k^+ + \frac{h_{k+1}}{2}A_k^- + \frac{h_k^2}{12}B_k^+ + \frac{h_{k+1}^2}{12}B_k^-, \qquad (3.32a)$$

$$Q_k = -\left(I^+ + \frac{h_k}{2}A_{k-1}^+ + \frac{h_k^2}{12}B_{k-1}^+\right), \qquad (3.32b)$$

$$R_k = -\left(I^- - \frac{h_{k+1}}{2}A_{k+1}^- + \frac{h_{k+1}^2}{12}B_{k+1}^-\right); \qquad (3.32c)$$

with

$$I^+ = \begin{bmatrix} 1 & 0 & 0 \\ 0 & 1 & 0 \\ 0 & 0 & 0 \end{bmatrix} \quad \textit{and} \quad I^- = \begin{bmatrix} 0 & 0 & 0 \\ 0 & 0 & 0 \\ 0 & 0 & 1 \end{bmatrix}.$$

In order to solve this system by Newton iteration, we need to linearize Eq. (3.31). If i denotes the number of the Newton iteration, then

$$\left(A_k\Psi^k\right)^{(i+1)} = \left(A_k\Psi^k\right)^{(i)} + \hat{A}_k\delta\Psi^k,$$
$$\left(B_k\Psi^k\right)^{(i+1)} = \left(B_k\Psi^k\right)^{(i)} + \hat{B}_k\delta\Psi^k,$$

where

$$\hat{A}_k = \begin{bmatrix} 0 & 0 & 1 \\ -\frac{v_k}{c_k} & -\frac{(f_k+c_k')}{c_k} & 0 \\ 0 & 1 & 0 \end{bmatrix},$$

$$\hat{B}_k = \begin{bmatrix} 0 & 1 & 0 \\ \frac{v_k}{c_k^2}(3c_k' + 2f_k) & \frac{f_k}{c_k^2}(3c_k' + f_k) - \frac{(c_k''+u_k)}{c_k} + 2\left(\frac{c_k'}{c_k}\right)^2 & \frac{v_k}{c_k} \\ -\frac{v_k}{c_k} & -\frac{(f_k+c_k')}{c_k} & 0 \end{bmatrix}.$$

Again we separate $\hat{A}_k$ and $\hat{B}_k$

$$\hat{A}_k^+ = \begin{bmatrix} 0 & 0 & 1 \\ -\frac{v_k}{c_k} & -\frac{(f_k+c_k')}{c_k} & 0 \\ 0 & 0 & 0 \end{bmatrix}, \qquad \hat{A}_k^- = \begin{bmatrix} 0 & 0 & 0 \\ 0 & 0 & 0 \\ 0 & 1 & 0 \end{bmatrix};$$

$$\hat{B}_k^+ = \begin{bmatrix} 0 & 1 & 0 \\ \frac{v_k}{c_k^2}(3c_k' + 2f_k) & \frac{f_k}{c_k^2}(3c_k' + f_k) - \frac{(c_k''+u_k)}{c_k} + 2\left(\frac{c_k'}{c_k}\right)^2 & \frac{v_k}{c_k} \\ 0 & 0 & 0 \end{bmatrix},$$

$$\hat{B}_k^- = \begin{bmatrix} 0 & 0 & 0 \\ 0 & 0 & 0 \\ -\frac{v_k}{c_k} & -\frac{(f_k+c_k')}{c_k} & 0 \end{bmatrix};$$

so that we now have the linear equation

$$\hat{R}_k \delta\Psi^{k+1} + \hat{P}_k \delta\Psi^k + \hat{Q}_k \delta\Psi^{k-1} = H_k \tag{3.33}$$

where $\hat{P}_k$, $\hat{Q}_k$ and $\hat{R}_k$ are defined from $\hat{A}_k$ and $\hat{B}_k$ as in (3.32) and

$$H_k = -\left(R_k \Psi^{k+1} + P_k \Psi^k + Q_k \Psi^{k-1}\right).$$

The boundary conditions (3.22) require the following modifications.

At the wall,

$$P_1 = \begin{bmatrix} 1 & 0 & 0 \\ 0 & 0 & 1 \\ \multicolumn{3}{c}{\text{same as } k \neq 1} \end{bmatrix}, \; R_1 = \begin{bmatrix} 0 & 0 & 0 \\ 0 & 0 & 0 \\ \multicolumn{3}{c}{\text{same as } k \neq 1} \end{bmatrix}, \; H_1 = \begin{bmatrix} 0 \\ 0 \\ \text{same} \end{bmatrix},$$

while, at the free stream,

$$P_J = \begin{bmatrix} \multicolumn{3}{c}{\text{same as } k \neq J} \\ \multicolumn{3}{c}{\text{same as } k \neq J} \\ 0 & 0 & 1 \end{bmatrix}, \; Q_J = \begin{bmatrix} \multicolumn{3}{c}{\text{same as } k \neq J} \\ \multicolumn{3}{c}{\text{same as } k \neq J} \\ 0 & 0 & 0 \end{bmatrix}, \; H_J = \begin{bmatrix} \text{same} \\ \text{same} \\ 0 \end{bmatrix}.$$

This system is solved by means of a block-tridiagonal factorization. Ψ^k is updated with $\delta\Psi^k$ and the process is repeated until convergence within preassigned tolerance is achieved.

Energy equation

For the energy equation (3.23) we follow the same steps as above (the linearization is unnecessary as Eqs. (3.23) are already linear):

$$\Psi_k = \begin{bmatrix} g_k \\ G_k \end{bmatrix}.$$

As Eqs.(3.24) are not homogeneous, we write

$$\frac{d\Psi^k}{dy} = A_k\Psi^k + \Phi_k \qquad and \qquad \frac{d^2\Psi^k}{dy^2} = B_k\Psi^k + \frac{d\Phi_k}{dy}$$

where

$$A_k = \begin{bmatrix} 0 & 1 \\ 0 & -\left(\frac{a_1'+f}{a_1}\right) \end{bmatrix}_k, \quad B_k = \begin{bmatrix} 0 & -\left(\frac{a_1'+f}{a_1}\right) \\ 0 & \frac{(a_1'+f)(2a_1'+f)-(a_1''+u)a_1}{{a_1}^2} \end{bmatrix}_k;$$

$$\Phi_k = \begin{bmatrix} 0 \\ -\frac{a_2'uv+a_2(uv'+v^2)}{a_1} \end{bmatrix}_k,$$

$$\frac{d\Phi_k}{dy} = \begin{bmatrix} 0 \\ -\frac{\left[a_2''uv+2a_2'(uv'+v^2)+a_2(uv''+3vv')\right]a_1-a_1'\left(a_2'uv+a_2(uv'+v^2)\right)}{a_1^2} \end{bmatrix}_k,$$

and

$$v' = -\frac{v}{c}(c'+f),$$
$$v'' = -\left(\frac{v'c-c'v}{c^2}\right)(c'+f) - \frac{v}{c}(c''+u).$$

We then separate A_k, B_k and Φ_k:

$$A_k^+ = \begin{bmatrix} 0 & 0 \\ 0 & -\left(\frac{a_1'+f}{a_1}\right) \end{bmatrix}_k, \qquad A_k^- = \begin{bmatrix} 0 & 1 \\ 0 & 0 \end{bmatrix},$$

$$B_k^+ = \begin{bmatrix} 0 & 0 \\ 0 & \frac{(a_1'+f)(2a_1'+f)-(a_1''+u)a_1}{{a_1}^2} \end{bmatrix}_k, \quad B_k^- = \begin{bmatrix} 0 & -\left(\frac{a_1'+f}{a_1}\right) \\ 0 & 0 \end{bmatrix}_k,$$

$$\Phi_k^+ = \Phi_k, \qquad \Phi_k^- = 0,$$

$$I^+ = \begin{bmatrix} 0 & 0 \\ 0 & 1 \end{bmatrix}, \qquad I^- = \begin{bmatrix} 1 & 0 \\ 0 & 0 \end{bmatrix}.$$

As for the momentum equations, the system can be written in the block - tridiagonal form

$$R_k \Psi^{k+1} + P_k \Psi^k + Q_k \Psi^{k-1} = H_k \tag{3.34}$$

where

$$P_k = I - \frac{h_k}{2} A_k^+ + \frac{h_{k+1}}{2} A_k^- + \frac{h_k^2}{12} B_k^+ + \frac{h_{k+1}^2}{12} B_k^-, \tag{3.35a}$$

$$Q_k = -\left(I^+ + \frac{h_k}{2} A_{k-1}^+ + \frac{h_k^2}{12} B_{k-1}^+ \right), \tag{3.35b}$$

$$R_k = -\left(I^- - \frac{h_{k+1}}{2} A_{k+1}^- + \frac{h_{k+1}^2}{12} B_{k+1}^- \right); \tag{3.35c}$$

and

$$H_k = \frac{h_k}{2}(\Phi_k^+ + \Phi_{k-1}^+) - \frac{h_k^2}{12}\left(\frac{d\Phi_k^+}{dy} - \frac{d\Phi_{k-1}^+}{dy} \right) - \frac{h_{k+1}}{2}(\Phi_{k+1}^- + \Phi_k^-) + \frac{h_{k+1}^2}{12}\left(\frac{d\Phi_{k+1}^-}{dy} - \frac{d\Phi_k^-}{dy} \right).$$

The boundary conditions (3.24) require the following special cases. At the wall,

$$P_1 = \begin{bmatrix} \text{same as } k \neq 1 & \\ 0 & 1 \end{bmatrix}, \quad R_1 = \begin{bmatrix} \text{same as } k \neq 1 & \\ 0 & 0 \end{bmatrix}, \quad H_1 = \begin{bmatrix} \text{same} \\ 0 \end{bmatrix}.$$

while, at the free stream,

$$P_J = \begin{bmatrix} 1 & 0 \\ \text{same as } k \neq J & \end{bmatrix}, \quad Q_J = \begin{bmatrix} 0 & 0 \\ \text{same as } k \neq J & \end{bmatrix}, \quad H_J = \begin{bmatrix} 1 \\ \text{same} \end{bmatrix}.$$

This system is solved by means of a block-tridiagonal factorisation.

4. Global Method

When no guess of the most-unstable eigenvalue is available, LINSTAB uses a global method that computes the entire eigenvalue spectrum. The second-order finite differenced compressible stability equations (3.13)-(3.17) can be reformulated as a matrix eigenvalue problem

$$\overline{A}\Phi = \omega \overline{B}\Phi, \tag{4.1}$$

where ω is the eigenvalue and Φ the discrete representation of the eigenfunctions

$$\Phi = \begin{bmatrix} \alpha\tilde{u} + \beta\tilde{w} \\ \tilde{v} \\ \tilde{p} \\ \tilde{T} \\ \alpha\tilde{w} - \beta\tilde{u} \end{bmatrix}. \tag{4.2}$$

The eigenvalues are the roots of the determinant equation

$$Det|\overline{A} - \omega\overline{B}| = 0. \tag{4.3}$$

This is a standard matrix eigenvalue problem and is solved using the complex 'shifted' LR method described in Wilkinson (1965).

The most unstable eigenvalue is the one with largest imaginary part. The global eigenvalue search is formulated so that no growing spurious modes (not physically relevant) are generated, see Malik (1982). The spurious modes are eliminated by using a finite–difference scheme for the eigenvalue analysis that is consistent with the scheme for the initial–value problem. When the eigenvalue problem (4.3) is solved using the complex LR algorithm, the storage requirements are $O(K^2)$ while the computational work is $O(K^3)$ where $K = 5N$ for the eighth order system. The global method is computationally expensive and should be used only when no guess of the eigenvalue is available.

All discrete eigenvalues obtained using complex 'shifted' LR method. The linear disturbance equations constitute an eigenvalue problem which yields the complex dispersion relation $\omega = \omega(\alpha, \beta)$ and the construction of this relation is the major concern of linear stability analysis.

5. Local Method

When a guess for the most-unstable eigenvalue is available, it can be improved by a local method which also computes the corresponding eigenfunction. In this section, we present two ways of numerically solving the compressible stability problem: inverse Rayleigh iteration and Newton iteration.

5.1 Inverse Rayleigh iteration

This procedure was used in the original version of LINSTAB, and its theory is presented in Wilkinson (1965). Generalization of this procedure to the compressible stability problem (3.13-3.17) results in the following algorithm

$$(\overline{A} - \omega_k \overline{B})\Phi^{(k+1)} = \overline{B}\Phi^{(k)} \tag{5.1}$$

$$(\overline{A} - \omega_k \overline{B})^T \Psi^{(k+1)} = \overline{B}^T \Psi^{(k)} \tag{5.2}$$

$$\omega_{k+1} = \frac{(\Psi^{(k+1)}, \overline{A}\Phi^{(k+1)})}{(\Psi^{(k+1)}, \overline{B}\Phi^{(k+1)})}. \tag{5.3}$$

The error satisfies $\omega_{k+1} - \omega = O((\omega_k - \omega)^3)$. The iteration cycle is started with the guessed eigenvalue produced by the global method, ω_0, and an assumed but arbitrary smooth profile for the eigenfunction $\Phi(0)$ and its adjoint $\Psi(0)$. The algorithm converges cubically for the eigenvalue, but the eigenfunction converges at the square root of this rate, as shown by Hackbusch (1985).

5.2 Newton iteration

Another method of local eigenvalue search to improve the accuracy of the most unstable eigenvalue is Newton iteration, which yields the same level of accuracy for the eigenfunction and the eigenvalue. In symbolic form, the system of ordinary differential equations satisfied by the linear disturbances can be written

$$\dot{L}\Phi = H, \tag{5.4}$$

where Φ is defined by eqn. (4.2) and $H = 0$. The boundary conditions for Eq. (5.4) are

$$\begin{cases} y = 0; & \phi_1 = \phi_2 = \phi_4 = \phi_5 = 0 \\ y \to \infty; & \phi_1, \phi_2, \phi_4, \phi_5 \to 0. \end{cases} \tag{5.5}$$

For the local eigenvalue problem, Eqs. (5.4) are a block-tridiagonal system which is solved using LU factorization. As Eq. (5.4) is homogeneous, in order to avoid a trivial solution, one inhomogeneous boundary conditions is imposed at the wall.

Specifically, as proposed by Malik (1990), the boundary condition $\phi_1(0) = 0$ is replaced by $\phi_3(0) = 1$. This is equivalent to normalizing the eigenfunction so that the pressure perturbation at the wall is unity. Since the pressure does not vanish at the wall, this condition is appropriate; see Malik (1990) for other possible normalizations. A non-trivial solution may now be obtained if $\omega = \omega_0$, the correct eigenvalue. Newton's method is used to iterate on ω until the missing boundary condition $\phi_1(0) = 0$ is satisfied. After a solution Φ is obtained using the estimated eigenvalue ω_0, the correction $\Delta\omega$ is determined from the linearized equation

$$\phi_1(0) + \frac{\partial \phi_1(0)}{\partial \omega} \Delta\omega = 0, \tag{5.6}$$

where $\phi_1(0)$ is known from the solution Φ just computed; $\partial\phi_1(0)/\partial\omega$ is obtained by solving

$$L\frac{\partial \Phi}{\partial \omega} = -\frac{\partial L}{\partial \omega}\Phi. \tag{5.7}$$

The process is repeated until $\phi_1(0)$ vanishes within a preassigned tolerance.

Boundary conditions

Homogeneous boundary conditions are used except for the pressure. The temperature perturbation is set to zero at the solid boundary. This is a reasonable assumption since high frequency disturbances do not penetrate into the wall due to thermal inertia. In other words, the wall appears insulated on the time scale of mean flow but not on the short time scales of the disturbances.

5.2.1 Second-order difference scheme

The second-order scheme used to discretize the linear disturbances equations (5.4) together with boundary conditions (5.5) is based on the following system of ordinary differential equations

$$(AD^2 + BD + C)\Phi = 0. \tag{5.8}$$

Here $D \equiv d/dy$, while A is given as

$$A = \begin{bmatrix} 1 & & & & 0 \\ & 1 & & & \\ & & 0 & & \\ & & & 1 & \\ 0 & & & & 1 \end{bmatrix}$$

and B and C are 5×5 matrices whose nonzero elements are given in Appendix I.

The system is discretized using second-order central differencing and leads to a block-tridiagonal system which is solved using a block LU elimination (Thomas algorithm).

5.2.2 Fourth-order compact difference scheme

To reach fourth-order accuracy we use the two-point compact difference scheme presented in Section *2.2.2*,

$$\Psi^k - \Psi^{k-1} = \frac{h_k}{2}\left(\frac{d\Psi^k}{dy} + \frac{d\Psi^{k-1}}{dy}\right) - \frac{h_k^2}{12}\left(\frac{d^2\Psi^k}{dy^2} - \frac{d^2\Psi^{k-1}}{dy^2}\right) + O(h_k^5), \qquad (5.9)$$

where $\Psi^k = \Psi(y_k)$ and $h_k = y_k - y_{k-1}$.

Using the continuity equation, the second-order normal momentum equation may be reduced to a first-order equation for pressure. Thus the linear stability equations (5.8) may be rewritten as a system of eight first-order equations

$$\frac{d\psi_i}{dy} = \sum_{j=1}^{8} a_{ij}\psi_j; \qquad i = 1, 2, ..., 8, \qquad (5.10)$$

where

$$\psi_1 = \alpha\tilde{u} + \beta\tilde{w}, \quad \psi_2 = \frac{d\psi_1}{dy}, \quad \psi_3 = \tilde{v}, \quad \psi_4 = \tilde{p},$$
$$\psi_5 = \tilde{T}, \quad \psi_6 = \frac{d\psi_5}{dy}, \quad \psi_7 = \alpha\tilde{w} - \beta\tilde{u}, \quad \psi_8 = \frac{d\psi_7}{dy}$$

with corresponding boundary conditions

$$\begin{cases} y = 0; & \psi_1 = \psi_3 = \psi_5 = \psi_7 = 0 \\ y \to \infty; & \psi_1, \psi_3, \psi_5, \psi_7 \to 0. \end{cases} \qquad (5.11)$$

The coefficients a_{ij} are given in Appendix II. In order to apply the compact scheme to Eq. (6.4), we also need

$$\frac{d^2\psi_i}{dy^2} = \sum_{j=1}^{8} b_{ij}\psi_j; \qquad i = 1, 2, ..., 8, \tag{5.12}$$

which is obtained by differentiating Eq. (4.10). Here

$$b_{ij} = \frac{da_{ij}}{dy} + \sum_{l=1}^{8} a_{il}a_{lj}$$

Thus Eq. (5.9) becomes

$$\psi_i^k - \frac{h_k}{2}\sum_{j=1}^{8} a_{ij}^k\psi_j^k + \frac{h_k^2}{12}\sum_{j=1}^{8} b_{ij}^k\psi_j^k - \left[\psi_i^{k-1} + \frac{h_k}{2}\sum_{j=1}^{8} a_{ij}^{k-1}\psi_j^{k-1} + \frac{h_k^2}{12}\sum_{j=1}^{8} b_{ij}^{k-1}\psi_j^{k-1}\right] = 0 \tag{5.13}$$

or

$$R_k\Psi^k + S_k\Psi^{k-1} = 0. \tag{5.14}$$

Eqs. (5.14) along with boundary conditions (5.11) are then written in the block-tridiagonal form

$$B_k\Psi^{k-1} + A_k\Psi^k + C_k\Psi^{k+1} = H, \tag{5.15}$$

where A_k, B_k, C_k are 8×8 matrices defined below and H is a 8×1 null matrix.

$$A_k = \left[\begin{array}{c} \text{last 4 rows of } \mathrm{R_k} \\ \hline \text{first 4 rows of } \mathrm{S_{k+1}} \end{array}\right]; \qquad k = 2, N-1, \tag{5.16}$$

$$B_k = \left[\begin{array}{c} \text{last 4 rows of } \mathrm{S_k} \\ \hline 0 \end{array}\right]; \qquad k = 2, N, \tag{5.17}$$

$$C_k = \left[\begin{array}{c} 0 \\ \hline \text{first 4 rows of } \mathrm{R_{k+1}} \end{array}\right]; \qquad k = 1, N-1, \tag{5.18}$$

$$A_1 = \left[\begin{array}{c} E \\ \hline \text{first 4 rows of } S_2 \end{array}\right], \tag{5.19}$$

$$A_N = \left[\begin{array}{c} \text{last 4 rows of } R_N \\ \hline F \end{array}\right], \tag{5.20}$$

where E and F are 4×8 matrices representing the bottom and top boundary conditions (4.11). Thus

$$E\Psi(0) = 0 \quad \text{and} \quad F\Psi(\infty) = 0, \tag{5.21}$$

where

$$E = \begin{bmatrix} 1 & 0 & 0 & 0 & 0 & 0 & 0 & 0 \\ 0 & 0 & 1 & 0 & 0 & 0 & 0 & 0 \\ 0 & 0 & 0 & 0 & 1 & 0 & 0 & 0 \\ 0 & 0 & 0 & 0 & 0 & 0 & 1 & 0 \end{bmatrix}, \tag{5.22}$$

and the elements of F are determined from the asymptotic behavior of Ψ as $y \to \infty$. For the details of the computation of F, see Malik (1982 - App. II) and Mack (1965, pp 266–271). As discussed above, the nonhomogeneous boundary conditions needed to avoid a trivial solution when solving system (5.15) is obtained by setting

$$E = \begin{bmatrix} 0 & 0 & 0 & 1 & 0 & 0 & 0 & 0 \\ 0 & 0 & 1 & 0 & 0 & 0 & 0 & 0 \\ 0 & 0 & 0 & 0 & 1 & 0 & 0 & 0 \\ 0 & 0 & 0 & 0 & 0 & 0 & 1 & 0 \end{bmatrix}, \tag{5.23}$$

and $H = (1, 0, 0, ..., 0)^T$.

The block-tridiagonal system (5.15) can now be solved by block-LU elimination.

5.2.3 Accuracy:

For a second order method,

$$\phi_h = \phi_{ex} + h^2\psi_1 + ...$$

$$\phi_{2h} = \phi_{ex} + 4h^2\psi_1 + ...$$

$\phi_{ex} = \frac{(4\phi_h - \phi_{2h})}{3}$ and truncation error ratio, $\varepsilon = \frac{(\phi_{ex} - \phi_{2h})}{(\phi_{ex} - \phi_h)} = 4$.

For a fourth order method,

$$\phi_h = \phi_{ex} + h^4\psi_1 + ...$$

$$\phi_{2h} = \phi_{ex} + 16h^4\psi_1 + ...$$

$\phi_{ex} = \frac{(16\phi_h - \phi_{2h})}{15}$ and truncation error ratio, $\varepsilon = \frac{(\phi_{ex} - \phi_{2h})}{(\phi_{ex} - \phi_h)} = 16$.

5.3.2 Group Velocity Computation

If (α, β) is the wave–vector, then group velocity is given by

$$\vec{V_g} = (\frac{\partial\omega}{\partial\alpha}, \frac{\partial\omega}{\partial\beta})$$

The compressible stability equations for three–dimensional disturbances are in the form

$$L(\alpha, \beta, \omega(\alpha, \beta))\vec{\phi} = 0.$$

After the above equation is differentiated with respect to ω, taking the inner product with the adjoint $\vec{\psi}$ of the eigenfunction $\vec{\phi}$ gives an expression for the group velocity. Since $(\vec{\psi}, L\frac{\partial\vec{\phi}}{\partial\alpha}) = (L^T\vec{\psi}, \frac{\partial\vec{\phi}}{\partial\alpha}) = 0$

$$\frac{\partial\omega}{\partial\alpha} = -\frac{(\vec{\psi}, \frac{\partial L}{\partial\alpha}\vec{\phi})}{(\vec{\psi}, \frac{\partial L}{\partial\omega}\vec{\phi})}$$

This method of computing the group velocity [Malik 1982] is more efficient than finite-differencing viz. $(\frac{\partial\omega}{\partial\alpha})_j = \frac{(\omega_{j+1} - \omega_{j-1})}{(\alpha_{j+1} - \alpha_{j-1})}$. The group velocity is obtained at less than 10% of the cost of the eigenvalue search.

6. Grid Adaptation

The grids used in linear stability analysis have a significant effect on the results. When the second-order accurate numerical scheme is used, the grids need to be very

smooth. In the original version of LINSTAB, exponentially stretched meshes were used, which are not well suited for grid adaptation.

By considering the truncation error inherent in finite-difference approximations, Vinokur (1983) proposed grid stretching functions based on the inverse hyperbolic sine. Besides being smooth, 'Vinokur' grids allow considerable control of the distribution of the points, which is not the case with exponentially stretched grids. The slopes at the wall and free-stream can be specified. It is also possible to join different Vinokur grids while retaining smoothness at the junctions. Finally, the number of grid points does not affect the shape of the grid. Several Vinokur grids were tried in the local computation. The resulting change in the eigenvalue ω is an indicator of how sensitive these computations are to the grid. This led us to implement an adaptive grid algorithm controlled by the error in the eigenfunctions.

Numerous adaptive grid methods are available. Most can be divided into two categories: displacement methods and refinement methods. The first type used a fixed number of mesh points and the adaptation consists of *moving* the mesh points from low-gradient regions to high-gradient regions. The second type starts with a coarse mesh and *adds* points in high-gradient regions. In an attempt to minimize the number of mesh-points, we first tried the displacement method based on a error equidistribution variational process proposed by Eiseman (1987). Although promising at low Mach number, this method was not able to handle the very steep gradients in the hypersonic second mode eigenfunctions, especially the temperature eigenfunction. The main cause was the inability of the algorithm to maintain the proper smoothness of the grid.

It was then decided to develop a grid-refinement method that would maintain the required mesh smoothness. The algorithm is defined by the following steps :

(i) The initial grids, G_0 and G_1, are Vinokur grids of 41 and 81 points;

(ii) The eigenfunctions computed on G_i and G_{i-1} are compared and estimates of the truncation error are constructed. Refinement intervals are introduced where the truncation error is greater than a specified ϵ;

(iii) The number of points on each refinement interval is doubled;

(iv) Smooth connection between new grids and the old ones is assured by a data-passing scheme;

(v) Repeat steps *(ii)* - *(iv)* until no more refinement intervals are found.

The main difficulty was the choice of interpolation method. To avoid the wiggles that appear with B-spline interpolation, we used the interpolation method based on piecewise cubic polynomials proposed by Akima (1970). The slope is determined using a second-order geometric rule which leads to very "natural looking" and smooth grids. The junctions between the old parts of the grid and the new parts generated with Akima's method were made from fifth-order B-splines.

When using a fourth-order accurate method, the smoothness requirement is less severe than for second-order methods, and thus Akima interpolation can be used everywhere.

This new method was first tested on a Mach 0.5 case for which the eigenfunctions are smooth. The iteration process converged rapidly (in less than 10 iterations) for $\epsilon \approx 10^{-5}$. For lower values of ϵ, the first 10 iterations simply doubled the points everywhere thus producing a huge number of grid points. This demonstrated the need for *early capture of the significant gradients.* Consequently, to obtain very low error (say $\epsilon \approx 10^{-7}$), we first need to converge for an intermediate value of ϵ and then restart the process on the resultant grid with a smaller value of ϵ.

Another option of the grid adaptation routine permits reduction of the number of points when a new structure has been captured, before continuing the adaptation process with a lower value of ϵ. This allows one to keep the number of grid points as low as possible while building some structure in the grid.

7. Results & Conclusions

Fourth–order accuracy is obtained both for the meanflow and the most unstable eigenfunction for the temporal stability problem. The advantage of this scheme is

the compact stencil which requires only two data points for fourth–order accuracy. It is also quite efficient compared to second–order methods requiring fewer grid points to resolve the flow accurately. These computations are not sensitive to the type of stretching functions like second–order computations.

Analysis of adjoint pressure eigenfunction indicates that the flow is sensitive to mass sources. The structure of the eigenfunctions is qualitatively different in different branches of the global eigenvalue spectrum. However, the modes investigated have a localized structure close to the wall.

Locally refining the grid using error estimates is a useful tool for ensuring accuracy of the eigenfunctions. Grid adaptation based on refinement shows better than power law convergence in the error.

The mean flow profiles for the compressible flat plate with an adiabatic wall were compared to the ones of Van Driest (1952). The quantities compared are the dimensionless boundary-layer thickness $\frac{\delta_{99\%}}{x}\sqrt{Re_x}$ and the mean skin-friction coefficient $C_f\sqrt{Re_x}$. Fig. 1 shows the boundary layer thickness quadratic dependence on Mach number for adiabatic wall conditions with fixed Reynolds and Prandtl numbers and edge temperature. The computed boundary layer thickness agrees quite well with the Van Driest curve.

Fig. 2 shows the effect of Mach number on non–dimensional skin–friction coefficient. The effect of increasing Mach number is to decrease the skin friction coefficient by about a factor of two as the Mach number increases from 0 to 20. The wall shear stress $[\tau_w = C_f M^2]$ increases.

Fig. 3 shows the meanflow for $M = 4.5, Re = 8000, Pr = 0.7$. The thermal boundary layer thickness is greater than velocity boundary layer thickness for Prandtl number less than unity. The adiabatic wall causes a bulge in the temperature profile since there is no heat transfer through the wall and viscous dissipation heats the flow in the near–wall region.

Fig. 4 shows the mean enthalpy profiles for $M = 4.5, Re = 8000, Pr = 0.7$ with isothermal and adiabatic wall conditions. For adiabatic wall conditions, the profile has zero slope at the wall and a bulge in the boundary layer as expected.

Fig. 5 shows the meanflow convergence history for $M = 4.5, Re = 8000$. The relative error is $\varepsilon = \max_j[|(1 - \frac{u_j}{u_{ex}})|]$ where u_{ex} is the exact solution of the discretized equations at grid point j and ε is the relative error. Typically the relative error drops one order of magnitude in per Newton iteration.

Fig. 6 shows the variation of mean flow error with number of grid points on a logarithmic scale for second and fourth order methods. The slopes are as expected.

Fig. 7 compares the efficiency of second order scheme to that of the fourth order compact scheme Newton iteration (N–R) for the mean flow calculation. For Re=2000, the fourth–order scheme gives reasonable accuracy with N=41 while for $N > 400$ is required for the second order scheme.

Fig. 8 shows that for a fourth order method, the ratio of errors on successive grids (number of grid points = 250, 500, 1000) higher more 16, indicating fourth order accuracy.

Fig. 9 shows the error distribution of mean flow enthalpy $\varepsilon_j = |(h_j - h_{ex})|$ for $M = 4.5, Re = 8000$. The error decreases by a factor of 2^4 for every grid doubling showing that the scheme is indeed fourth order accurate. The error curves collapse when scaled appropriately. The dip in the absolute error is due to a sign change.

Fig. 10 shows that the global eigenvalue spectrum has two branches. The number of eigenvalues increases with increasing grid resolution. The structure of eigenfunctions is different in each branch. The eigenfunction structure in the two branches is investigated.

Figs. 11 and 12 show the eigenvalue structure in two branches of the global eigenvalue spectrum. In the mode shown in fig. 11 for $\lambda = (1.085, -0.555)$, the structure is localized close to the wall while the mode in figure 12 for the eigenvalue $\lambda = (0.585, 25.93)$ is highly oscillatory.

Fig. 13 shows the non-dimensionalized pressure and its adjoint eigenfunction structure. At Re=8000 and M=4.5, the pressure adjoint is about 4 orders of magnitude higher indicating that the flow is sensitive to mass sources or errors equivalent to mass sources.

Fig. 14 shows the temperature and its adjoint eigenfunction structure. At Re=8000 and M=4.5, the structure is quite confined close to the wall.

Fig. 15 gives the discretization error of the most unstable eigenvalue of the second and fourth order schemes using local search. If $(\lambda_r^{ex}, \lambda_i^{ex})$, $(\lambda_r^j, \lambda_i^j)$ are the most unstable eigenvalues of the discretized equations and on a grid j, then $\varepsilon = \sqrt{(\lambda_r^{ex} - \lambda_r^j)^2 + (\lambda_i^{ex} - \lambda_i^j)^2}$

Fig. 16 shows the comparison of the discretized error (accuracy) in the most unstable eigenvalue computed by the fourth order compact Newton iteration for exponential and Vinokur stretching functions. Exponential stretching appears to give slightly higher accuracy for the same number of grid points.

Fig. 17 shows the CPU time vs. accuracy for inverse Rayleigh iteration on a SPARC-10 station.

Fig. 18 shows the CPU time for global and local calculations on C-90. The cost of the global method scales as N^3 while, for the local method, it increases as N, where N is the number of grid points.

Fig. 19 shows that the real part of group velocity increases linearly with Mach number while the imaginary part seems to decrease with M for $Re = 8000, \alpha = 2.25, \beta = 0$.

Fig. 20 shows the comparison of an estimate of the absolute maximum error with and without refinement for the mean flow. The adaptive grid error decreases faster than exponentially.

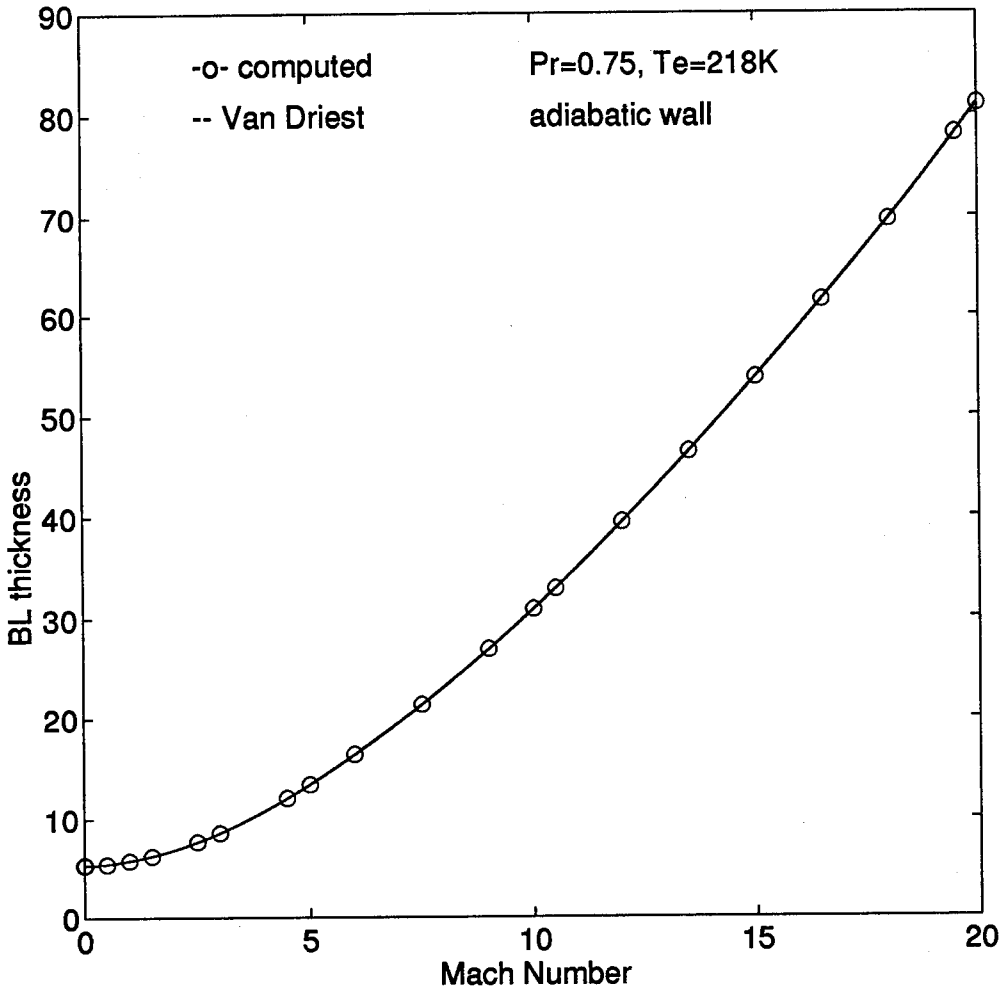
-o- computed
-- Van Driest
Pr=0.75, Te=218K
adiabatic wall
BL thickness
Mach Number
0
10
20
30
40
50
60
70
80
90
0
5
10
15
20

FIGURE 1

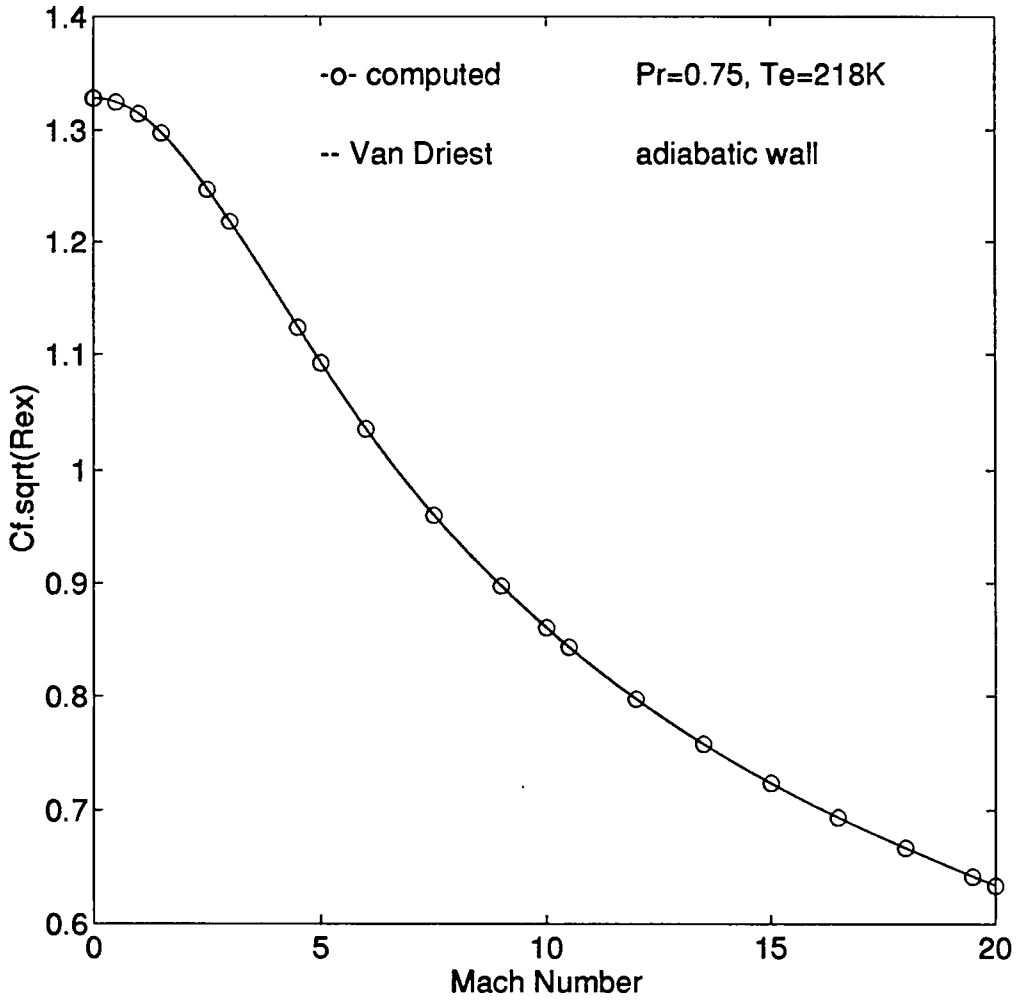
-o- computed
Pr=0.75, Te=218K
-- Van Driest
adiabatic wall
Cf.sqrt(Rex)
Mach Number
1.4
1.3
1.2
1.1
1
0.9
0.8
0.7
0.6
0
5
10
15
20

FIGURE 2

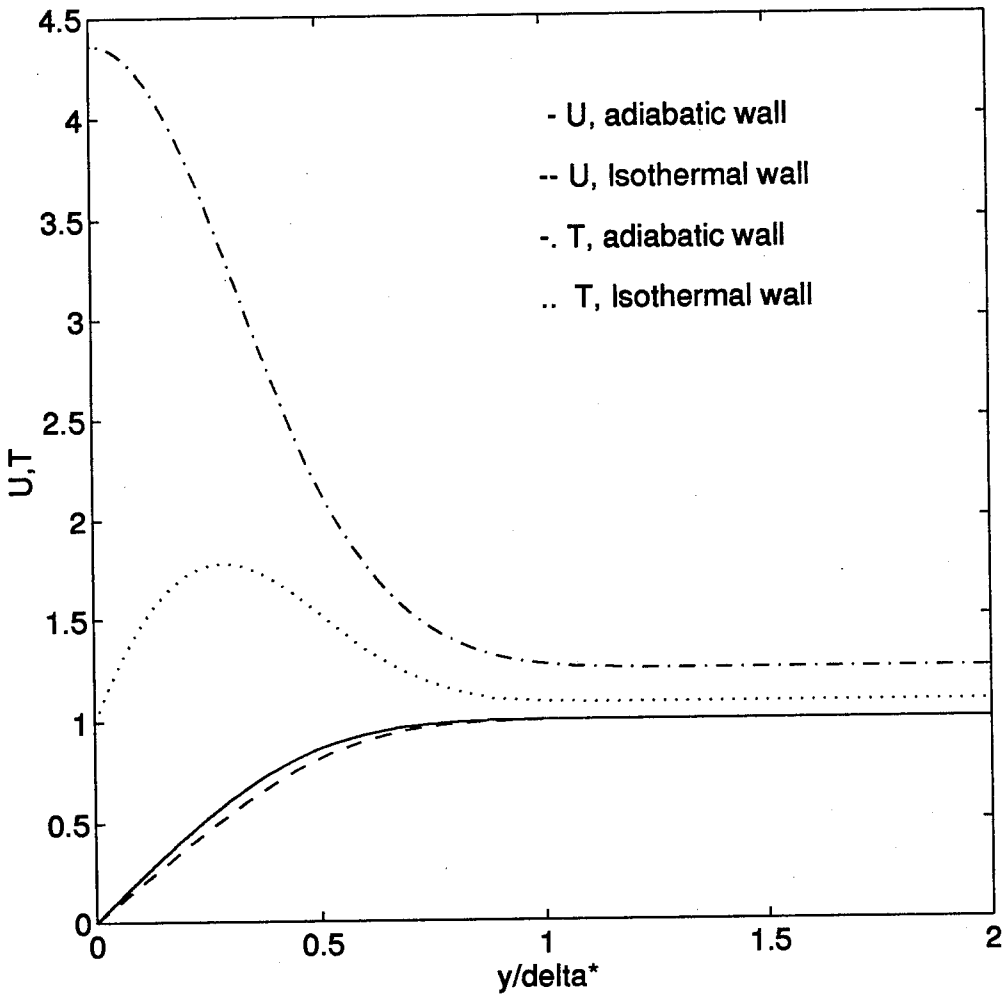
4.5
4
3.5
3
2.5
2
1.5
1
0.5
0
U,T
0
0.5
1
1.5
2
y/delta*
- U, adiabatic wall
-- U, Isothermal wall
-. T, adiabatic wall
.. T, Isothermal wall

FIGURE 3

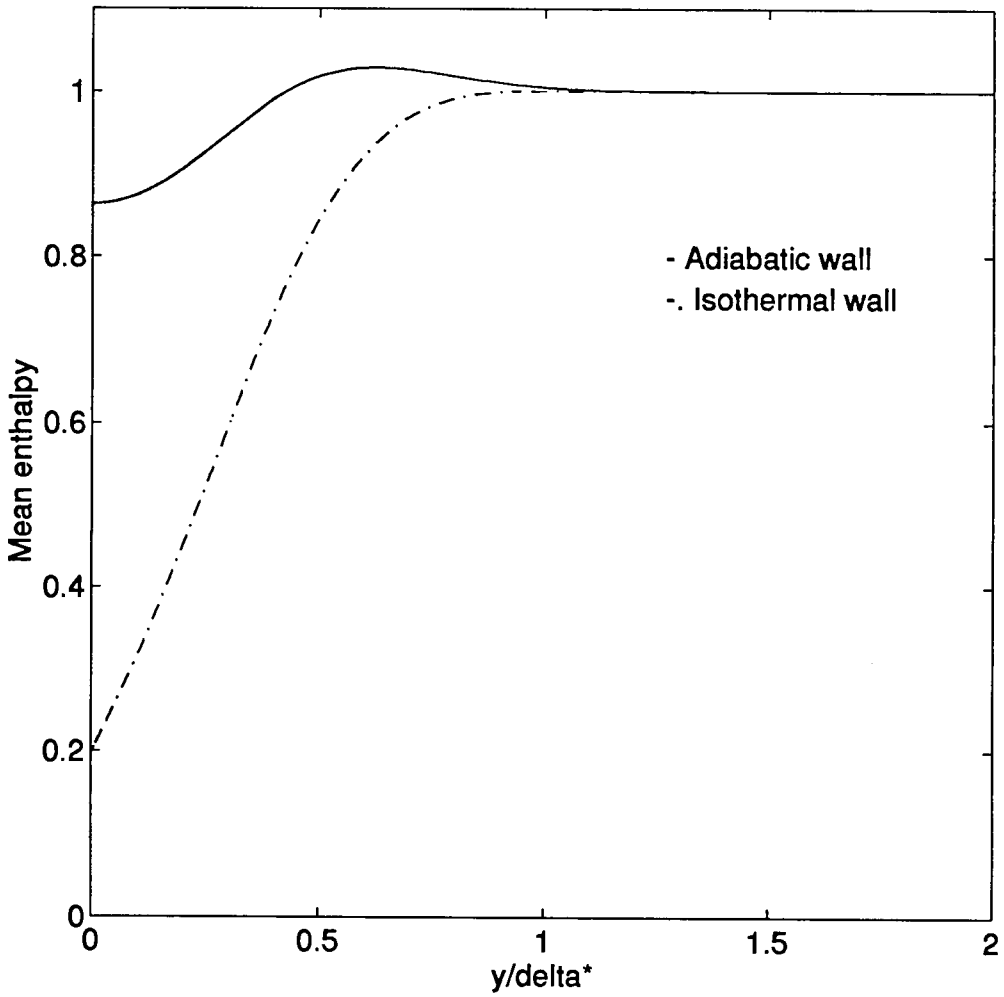
Mean enthalpy
y/delta*
- Adiabatic wall
-. Isothermal wall
0
0.2
0.4
0.6
0.8
1
0
0.5
1
1.5
2

FIGURE 4

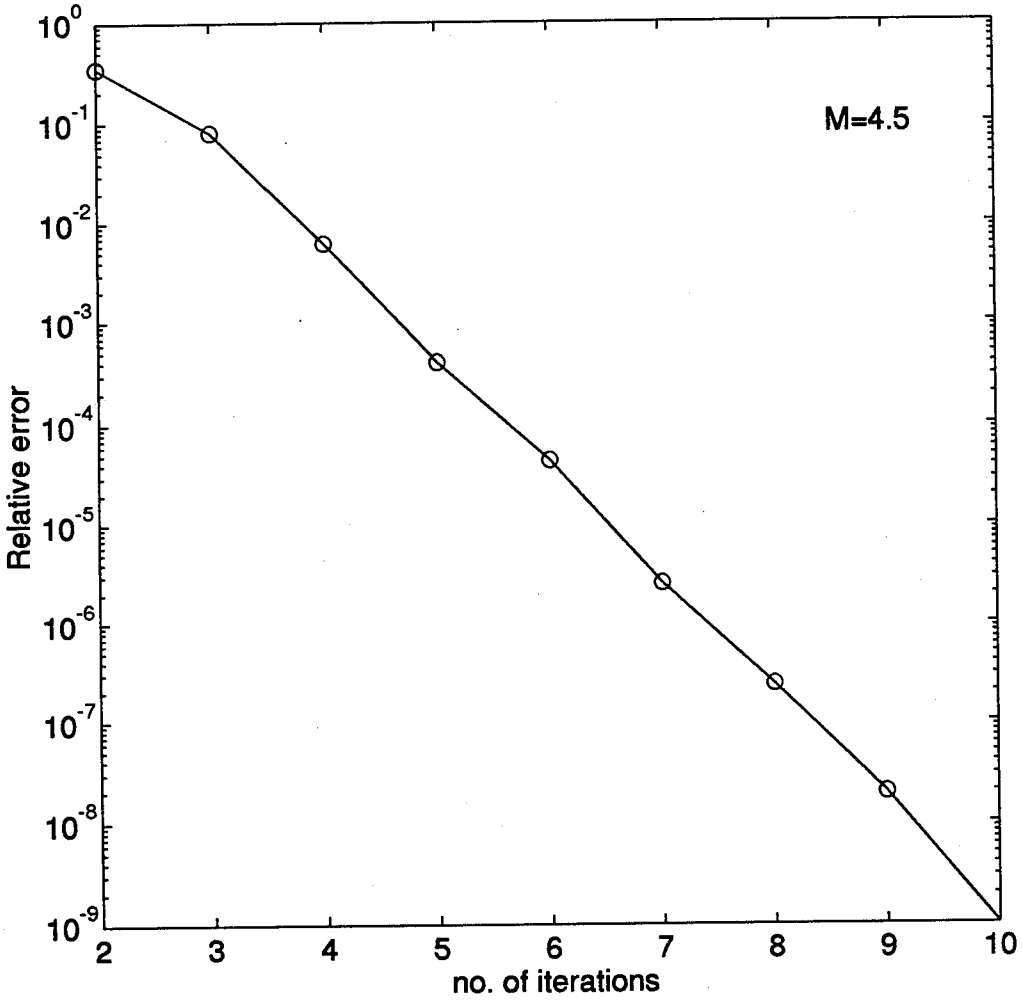
M=4.5
Relative error
no. of iterations
10^{0}
10^{-1}
10^{-2}
10^{-3}
10^{-4}
10^{-5}
10^{-6}
10^{-7}
10^{-8}
10^{-9}
2
3
4
5
6
7
8
9
10

FIGURE 5

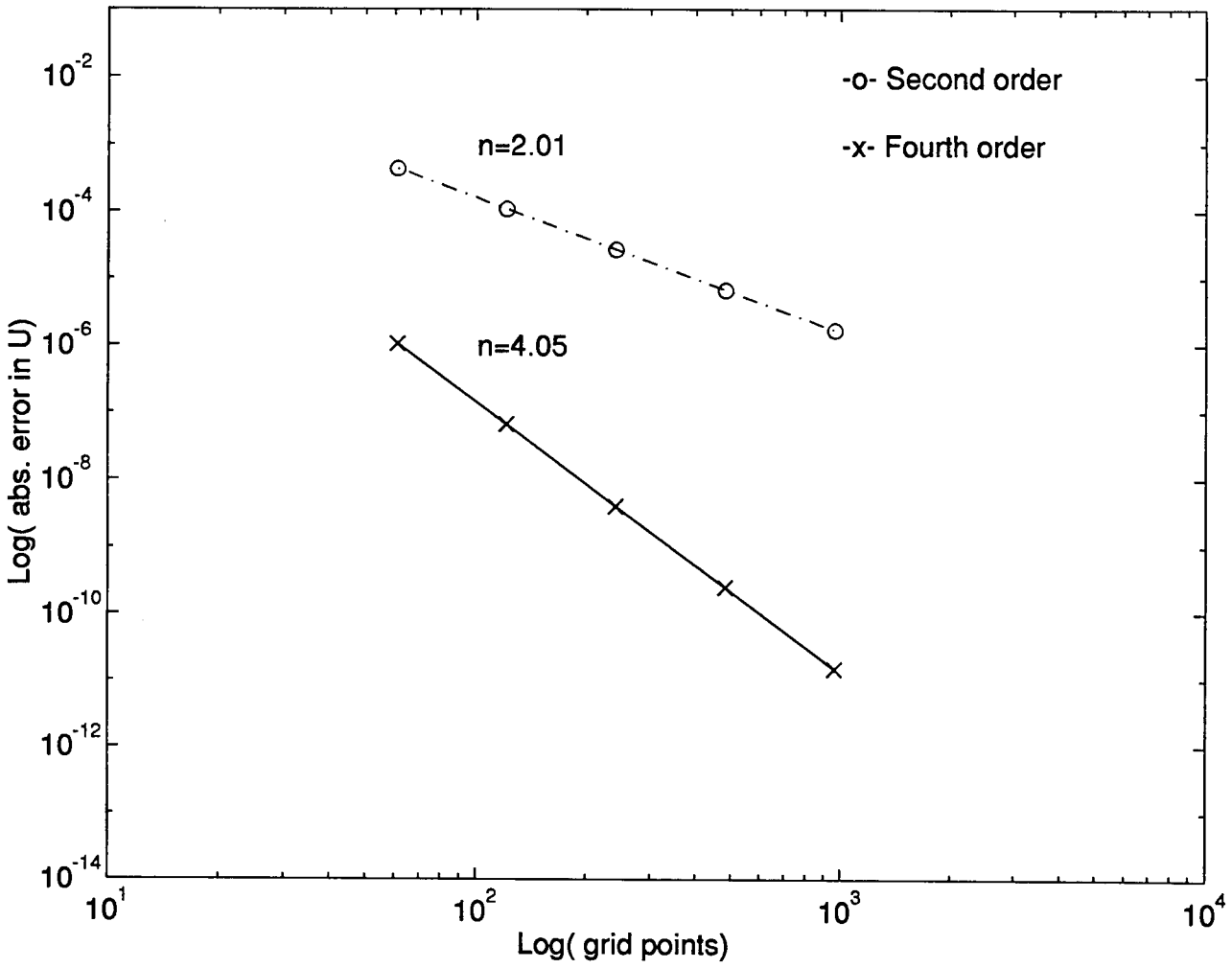
-o- Second order
-x- Fourth order
n=2.01
n=4.05
Log(abs. error in U)
Log(grid points)
10^-2
10^-4
10^-6
10^-8
10^-10
10^-12
10^-14
10^1
10^2
10^3
10^4

FIGURE 6

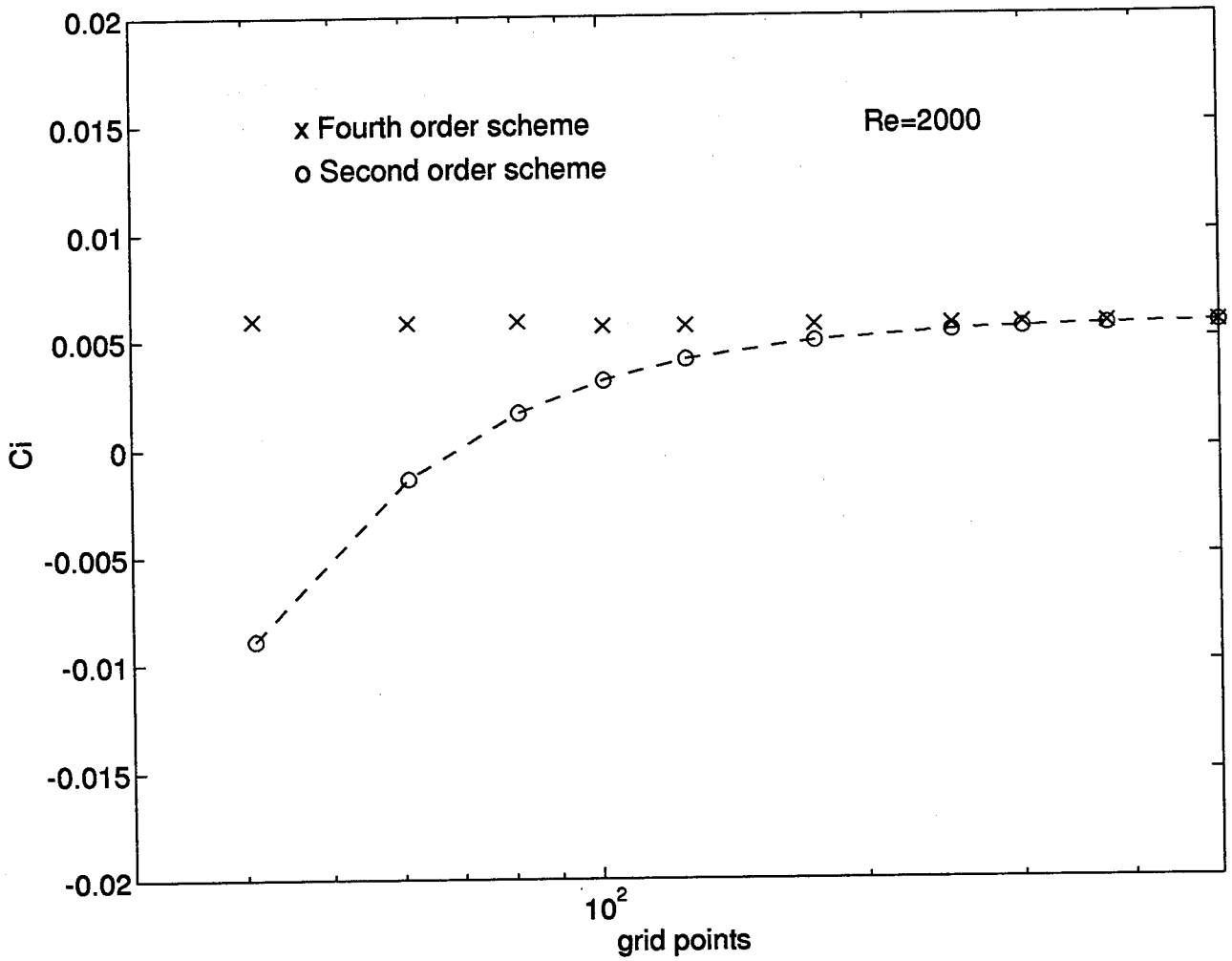
0.02
0.015
0.01
0.005
0
-0.005
-0.01
-0.015
-0.02
Ci
x Fourth order scheme
o Second order scheme
Re=2000
10^2
grid points

FIGURE 7

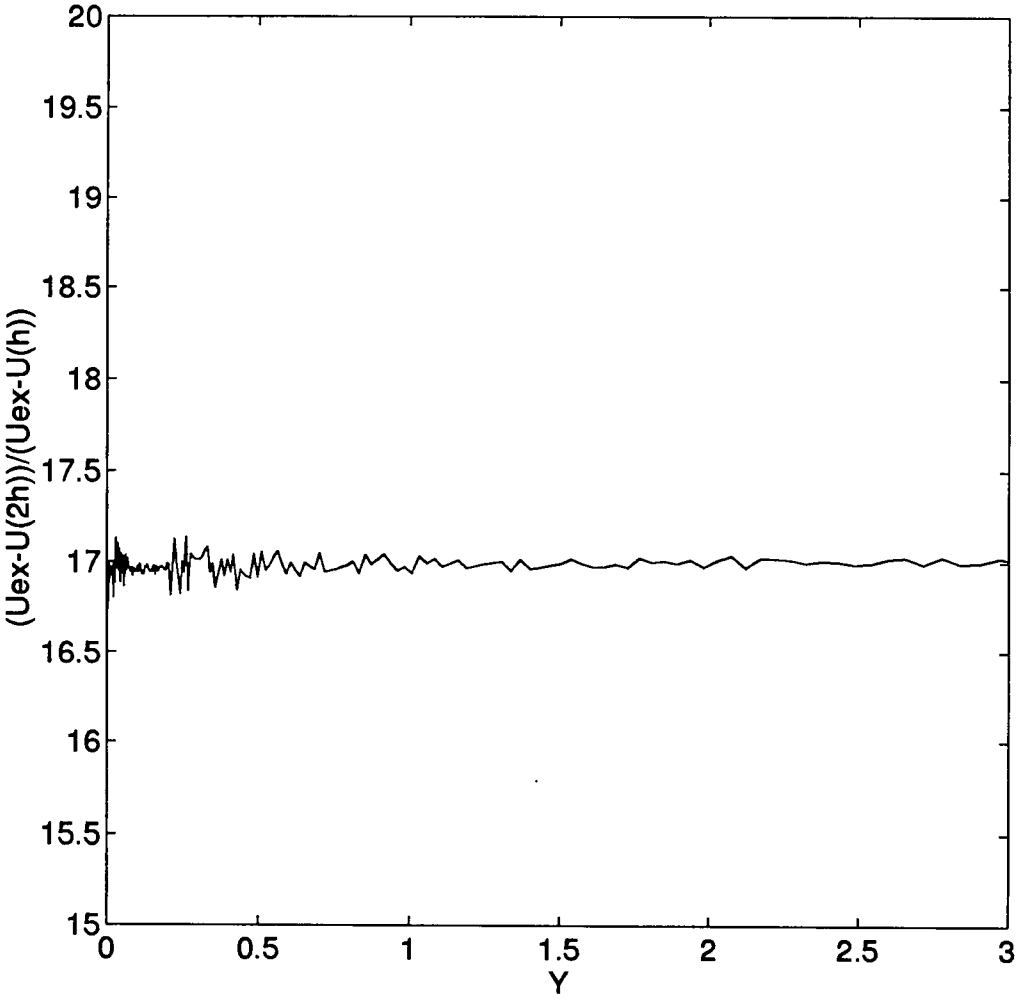

FIGURE 8

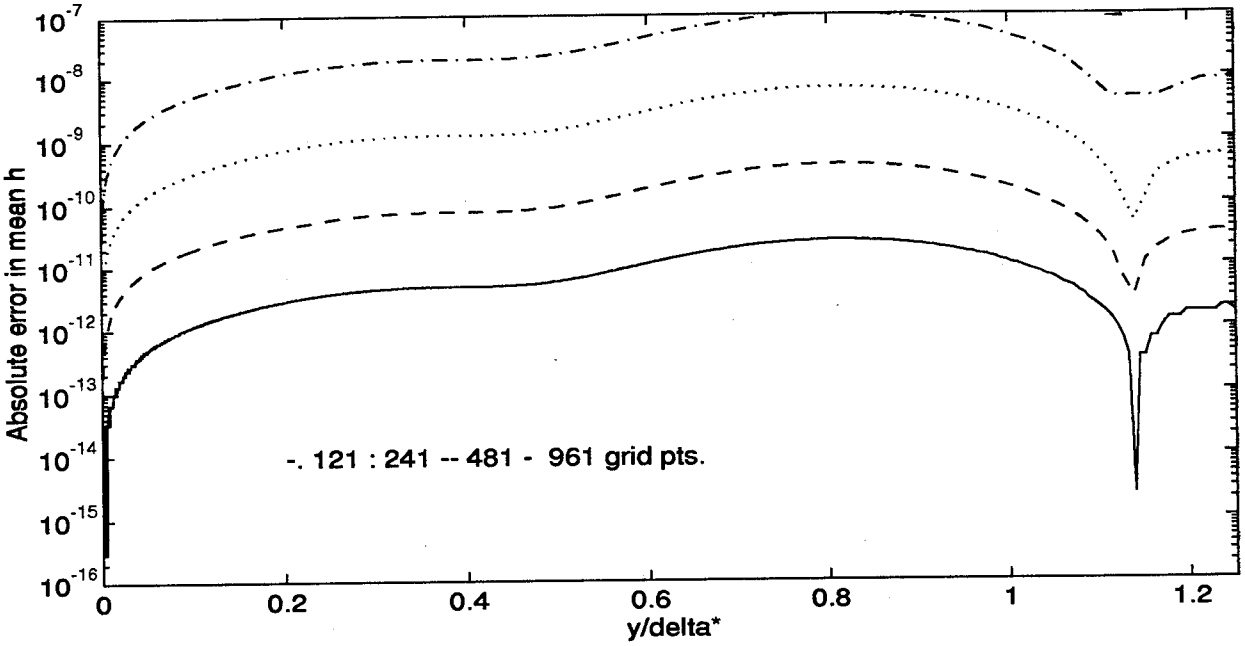
Absolute error in mean h
y/delta*
-. 121 : 241 -- 481 - 961 grid pts.

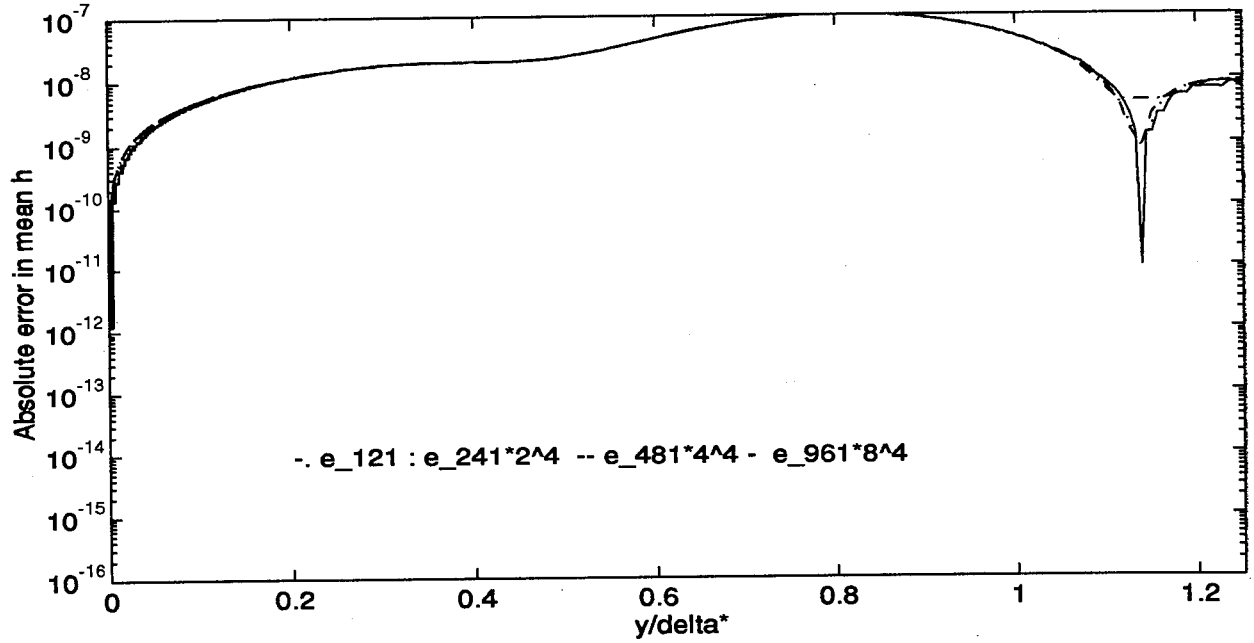
Absolute error in mean h
y/delta*
-. e_121 : e_241*2^4 -- e_481*4^4 - e_961*8^4

FIGURE 9

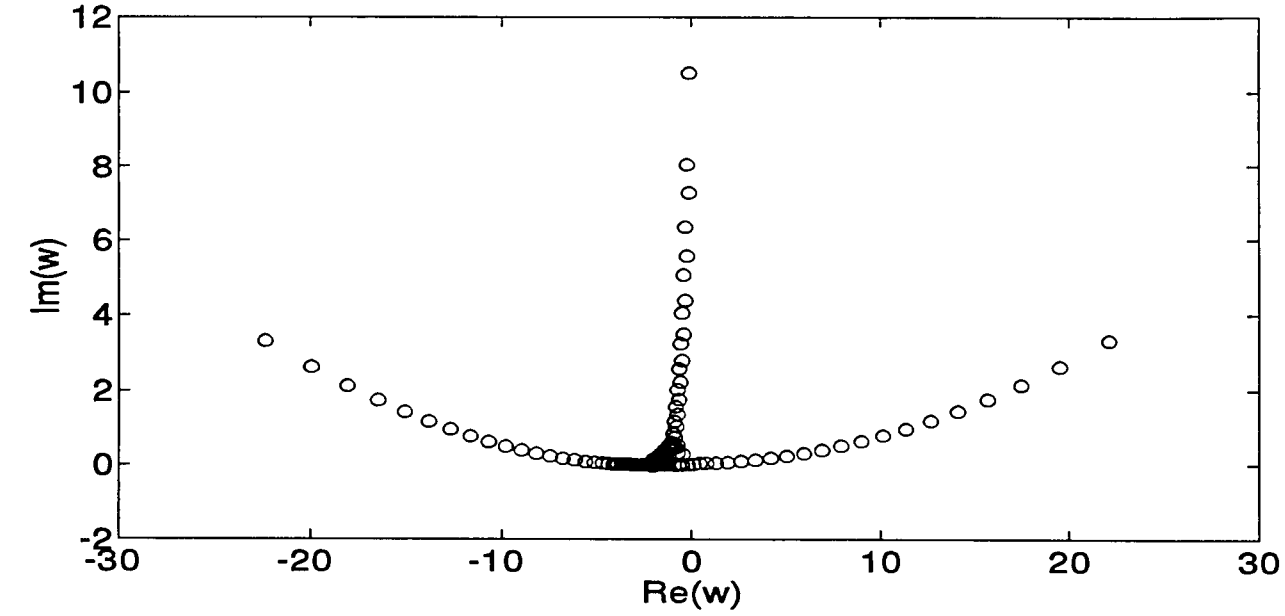

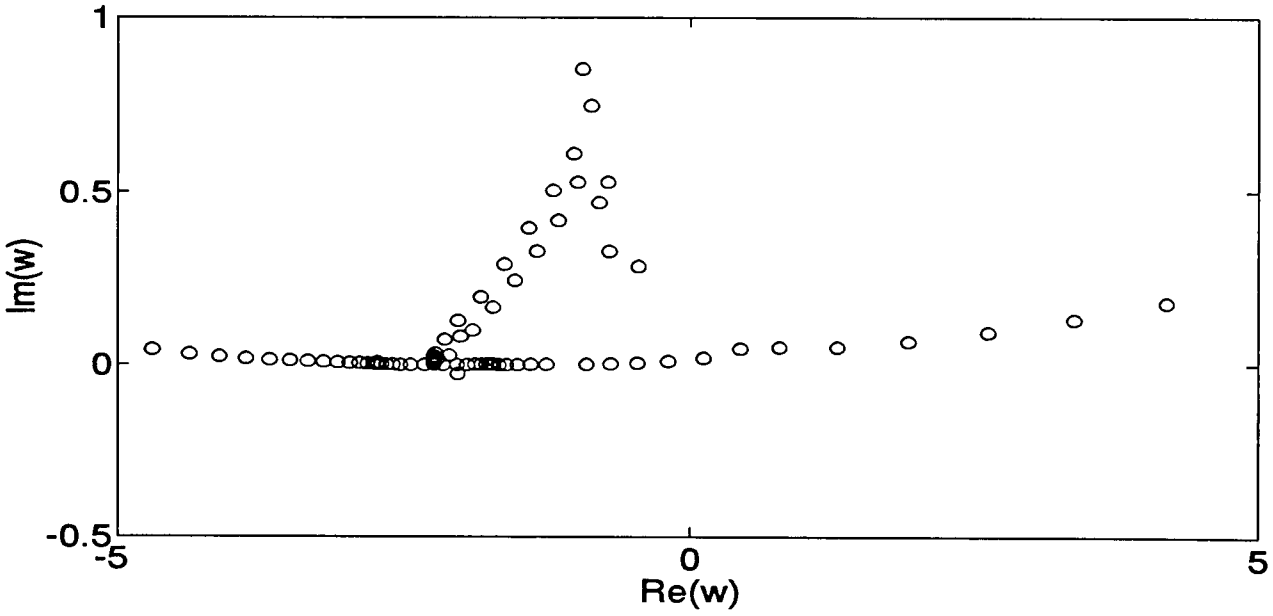

FIGURE 10

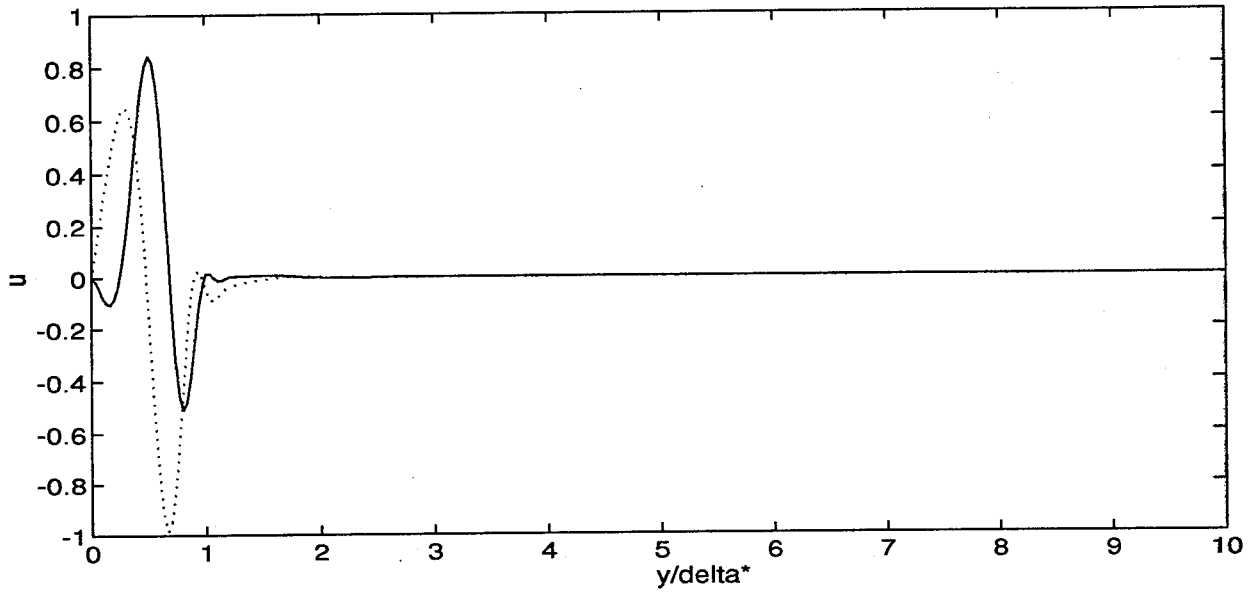

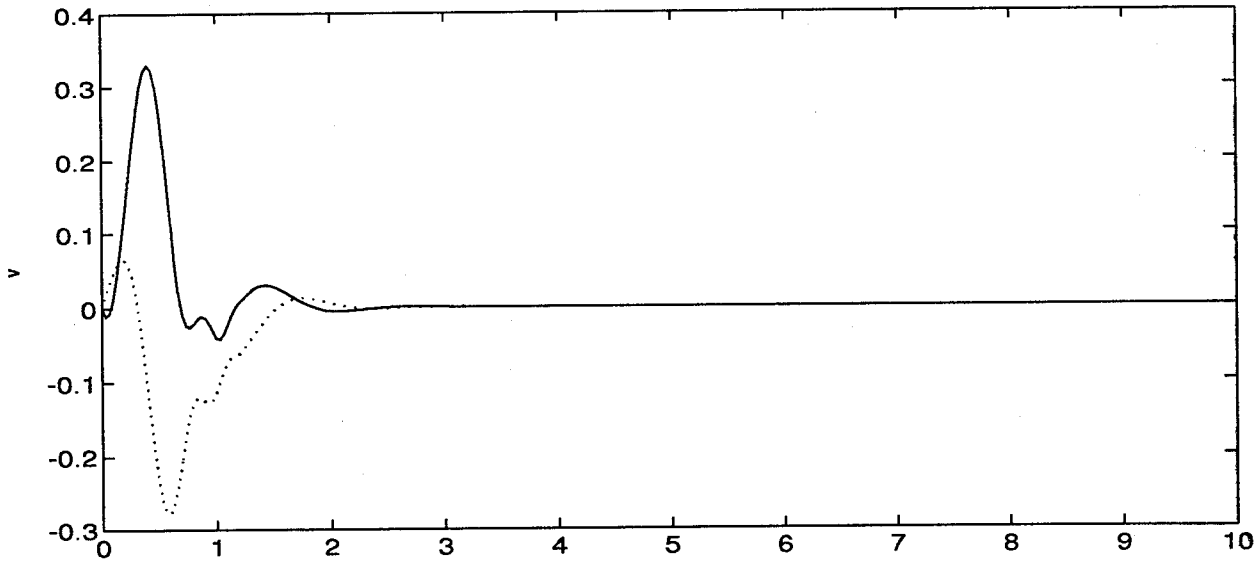

FIGURE 11

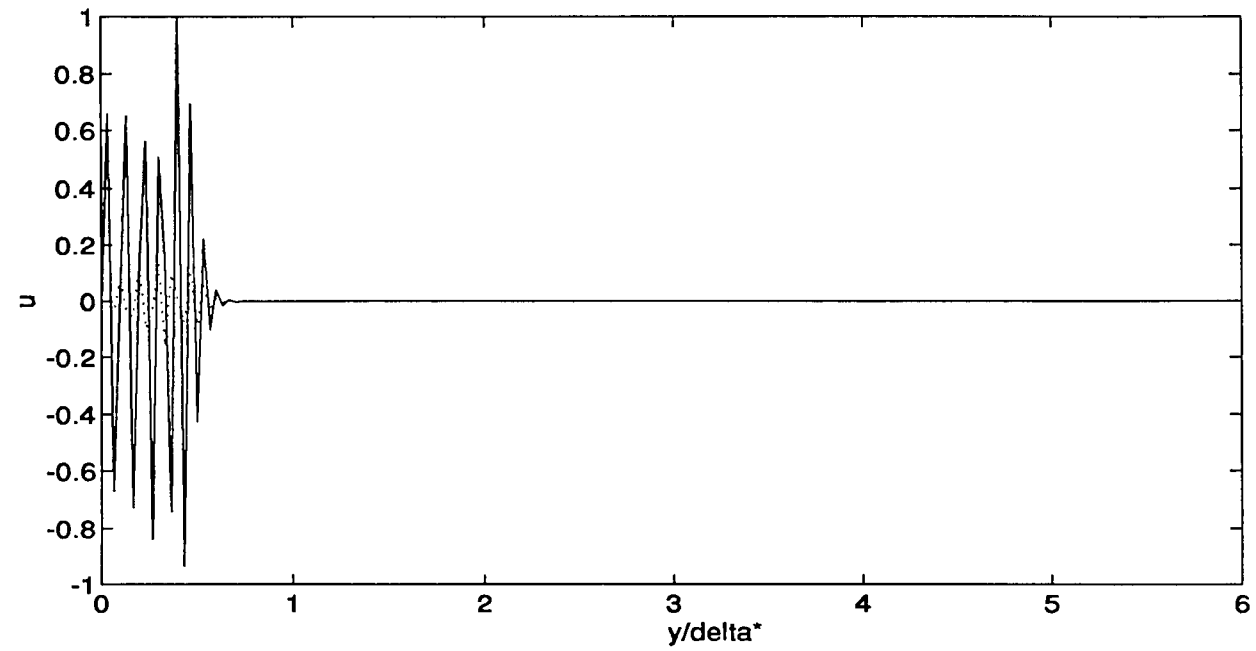
1
0.8
0.6
0.4
0.2
0
-0.2
-0.4
-0.6
-0.8
-1
u
0
1
2
3
4
5
6
y/delta*

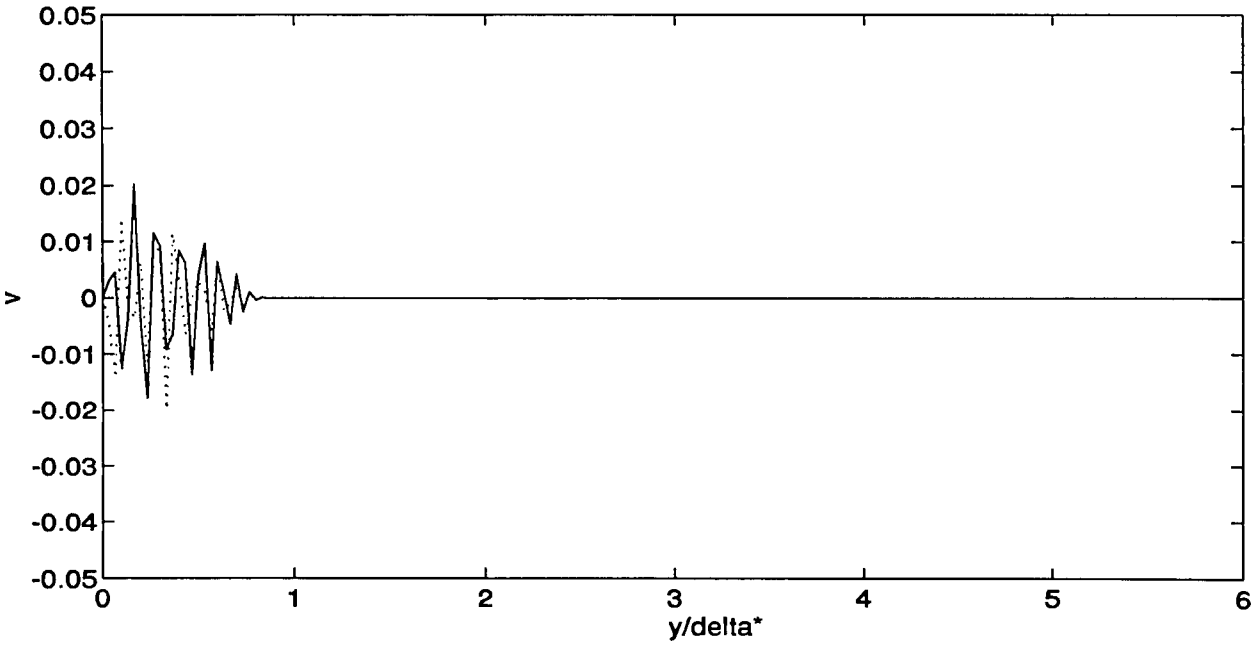
0.05
0.04
0.03
0.02
0.01
0
-0.01
-0.02
-0.03
-0.04
-0.05
v
0
1
2
3
4
5
6
y/delta*

FIGURE 12

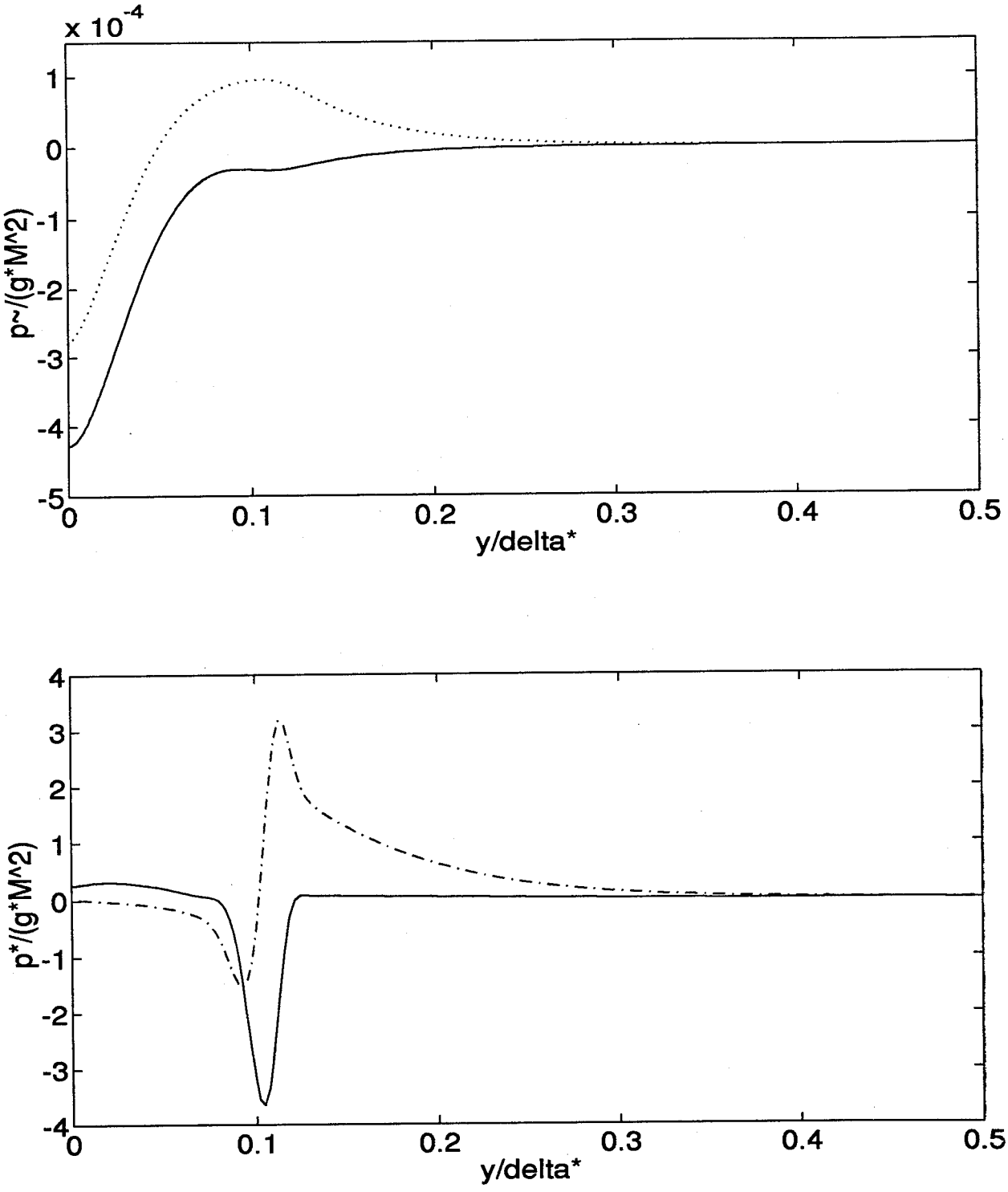
x 10^-4
1
0
-1
-2
-3
-4
-5
p~/(g*M^2)
0
0.1
0.2
0.3
0.4
0.5
y/delta*
4
3
2
1
0
-1
-2
-3
-4
p*/(g*M^2)
0
0.1
0.2
0.3
0.4
0.5
y/delta*

FIGURE 13

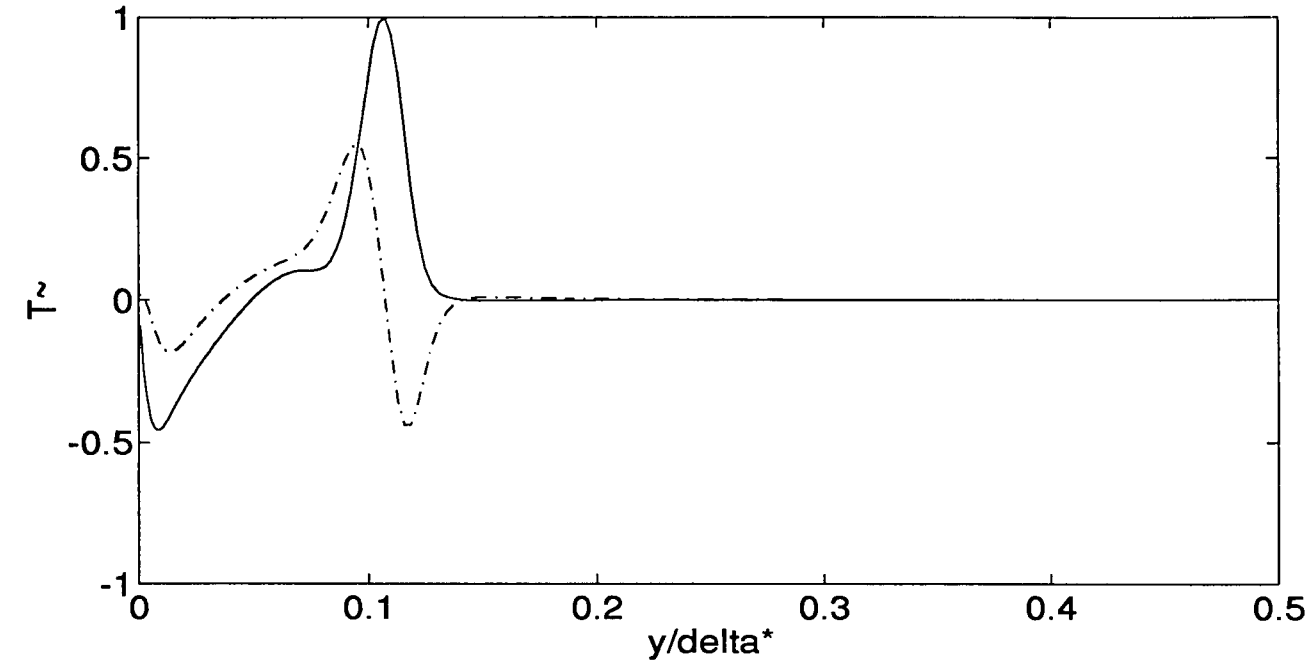
1
0.5
0
-0.5
-1
T~
0
0.1
0.2
0.3
0.4
0.5
y/delta*

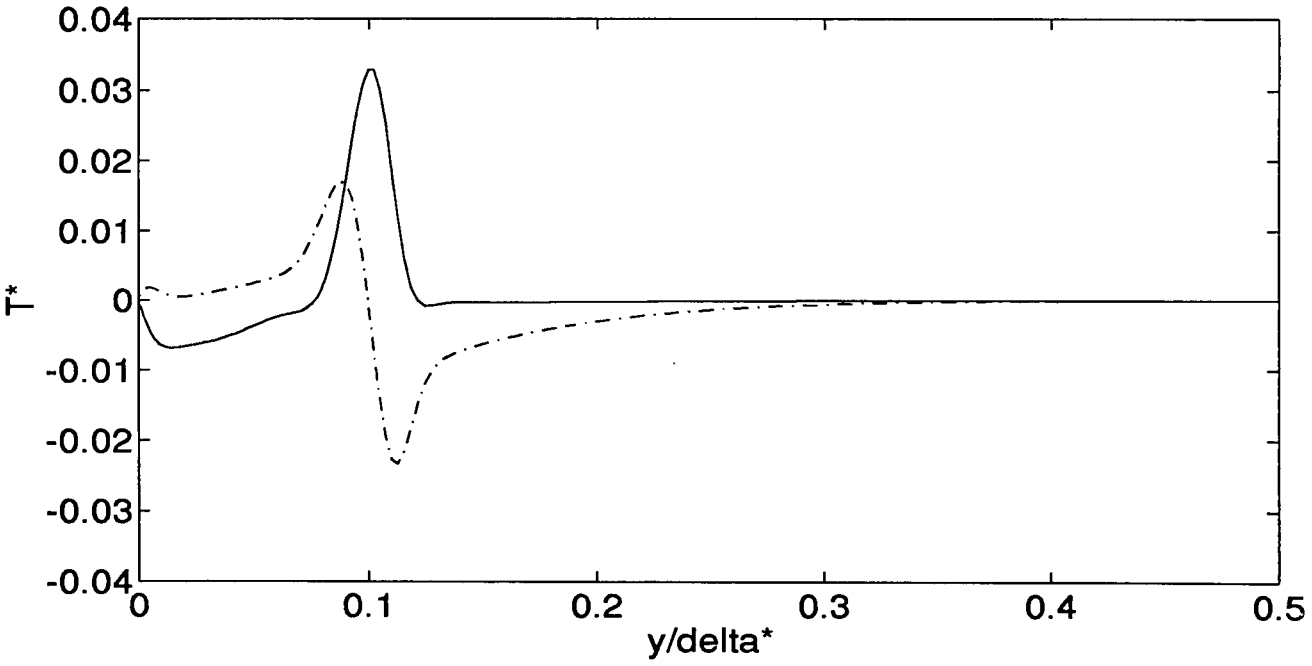
0.04
0.03
0.02
0.01
0
-0.01
-0.02
-0.03
-0.04
T*
0
0.1
0.2
0.3
0.4
0.5
y/delta*

FIGURE 14

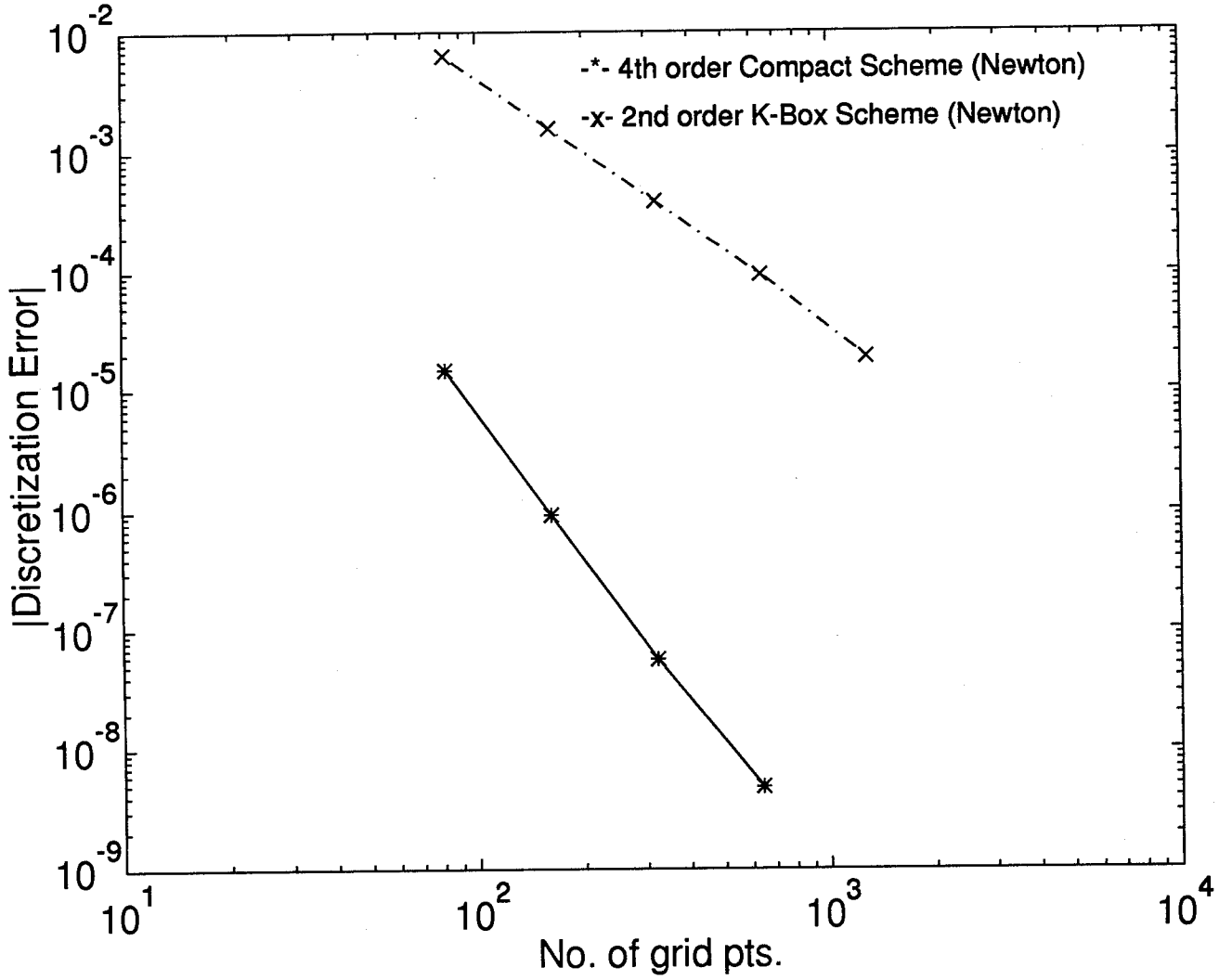
-*- 4th order Compact Scheme (Newton)
-x- 2nd order K-Box Scheme (Newton)
|Discretization Error|
No. of grid pts.
10^-2
10^-3
10^-4
10^-5
10^-6
10^-7
10^-8
10^-9
10^1
10^2
10^3
10^4

FIGURE 15

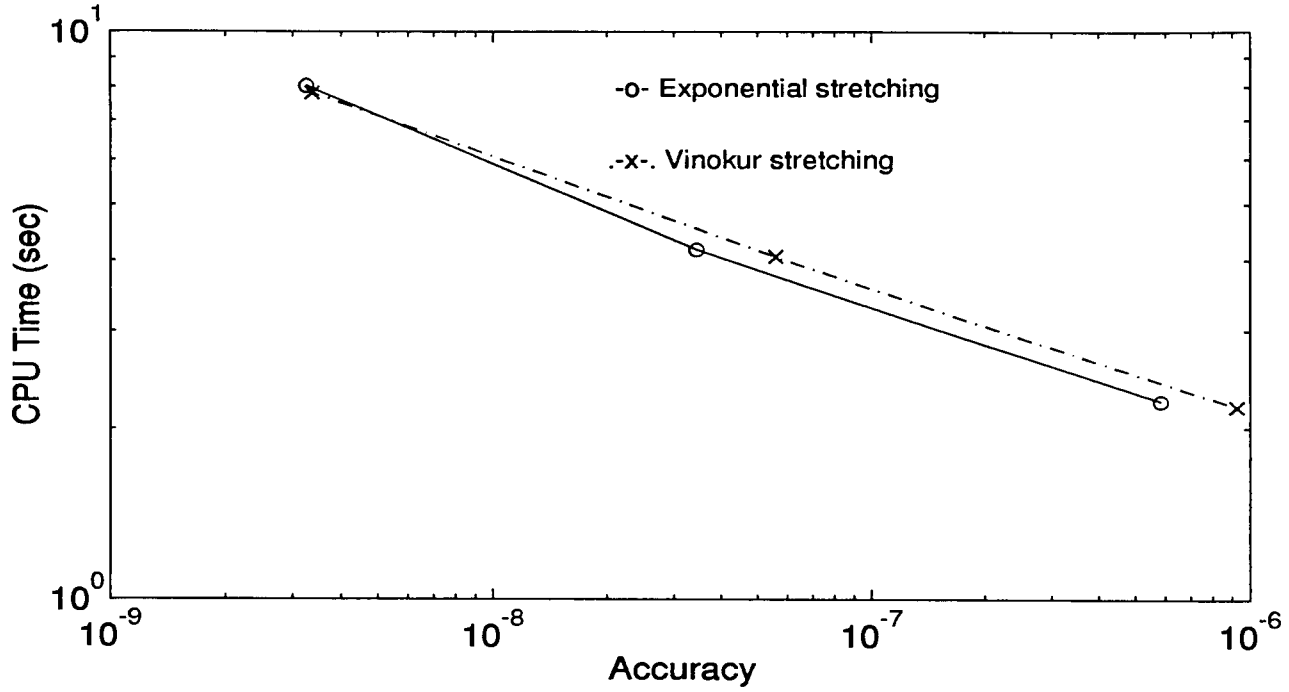
-o- Exponential stretching
.-x-. Vinokur stretching
CPU Time (sec)
Accuracy
10^1
10^0
10^-9
10^-8
10^-7
10^-6

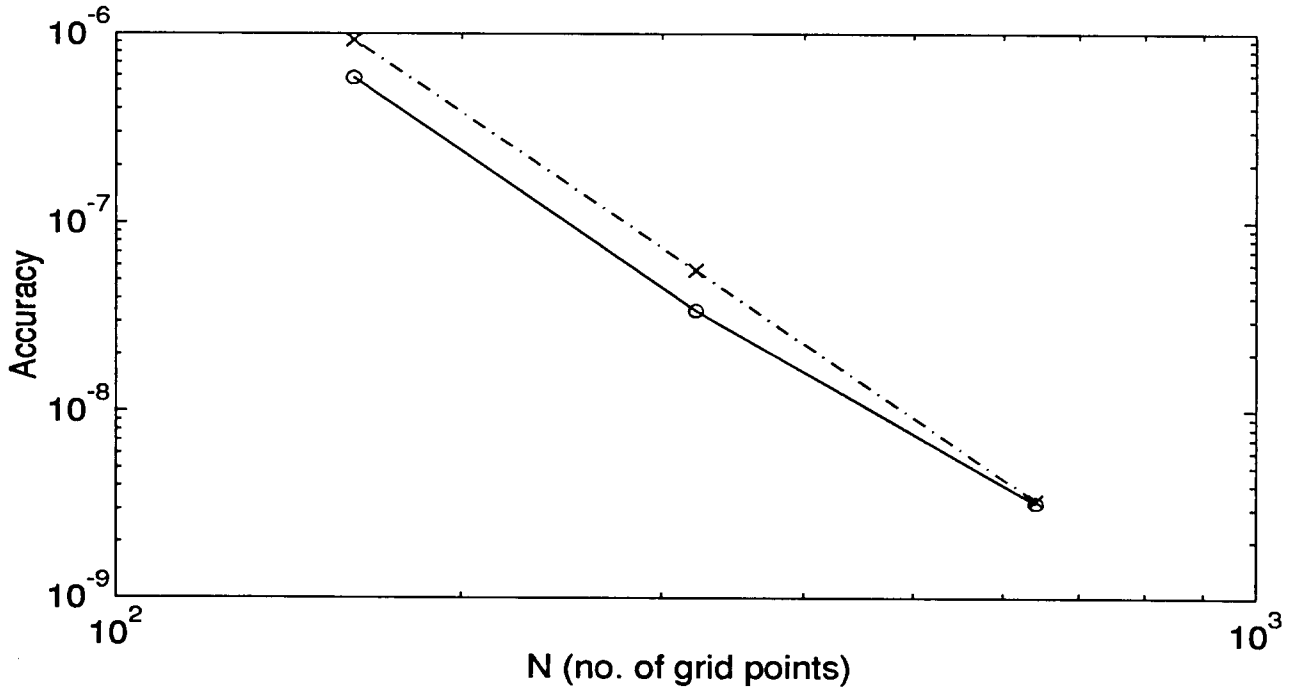
Accuracy
N (no. of grid points)
10^-6
10^-7
10^-8
10^-9
10^2
10^3

FIGURE 16

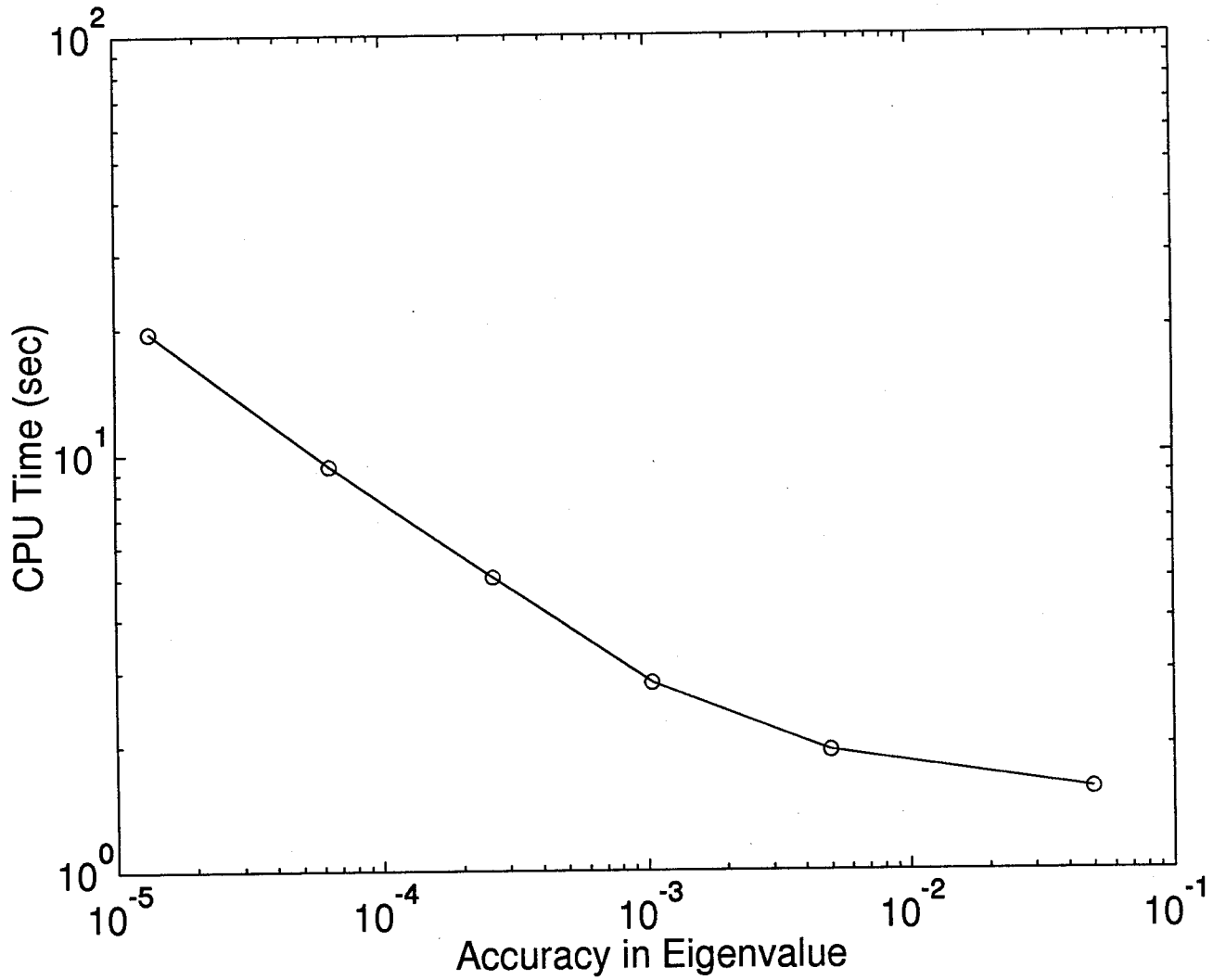
10^2
10^1
10^0
CPU Time (sec)
10^{-5}
10^{-4}
10^{-3}
10^{-2}
10^{-1}
Accuracy in Eigenvalue

FIGURE 17

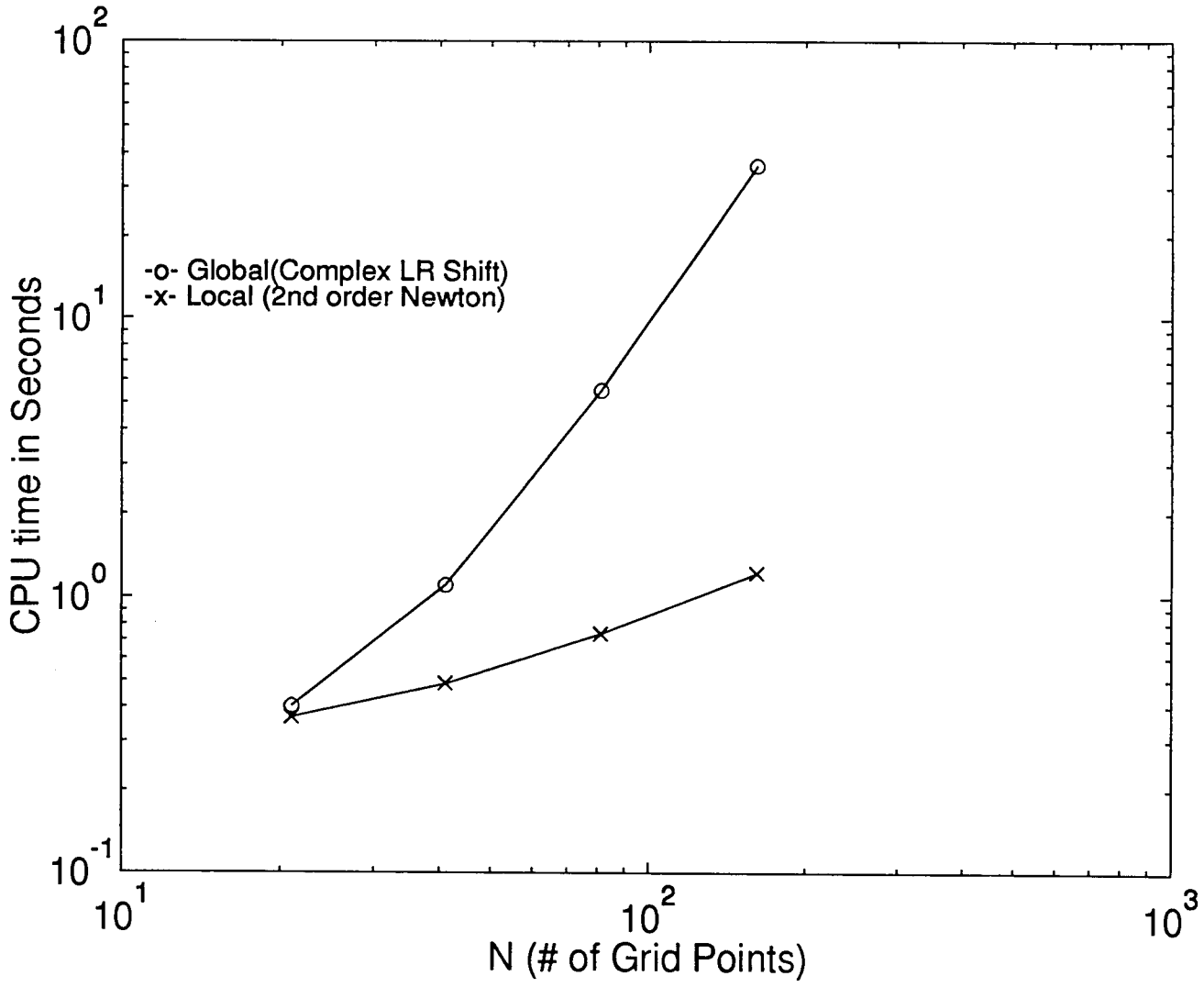
10^2
10^1
10^0
10^{-1}
CPU time in Seconds
-o- Global(Complex LR Shift)
-x- Local (2nd order Newton)
10^1
10^2
10^3
N (# of Grid Points)

FIGURE 18

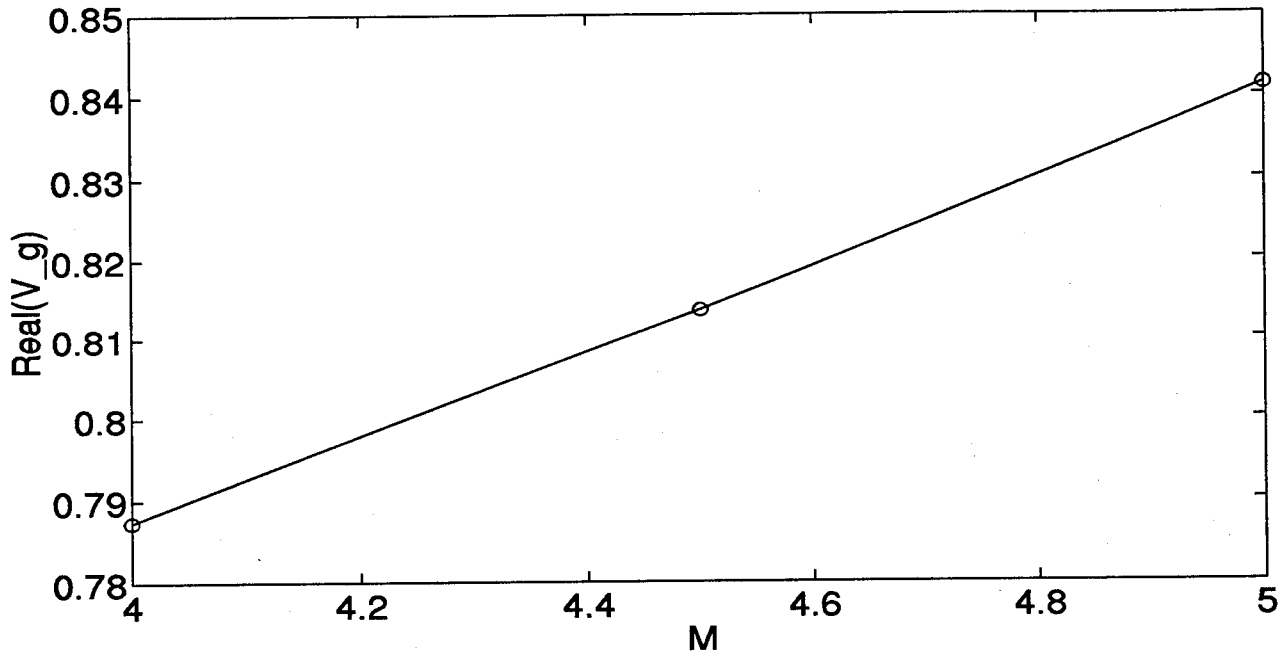
0.85
0.84
0.83
0.82
0.81
0.8
0.79
0.78
Real(V_g)
4
4.2
4.4
4.6
4.8
5
M

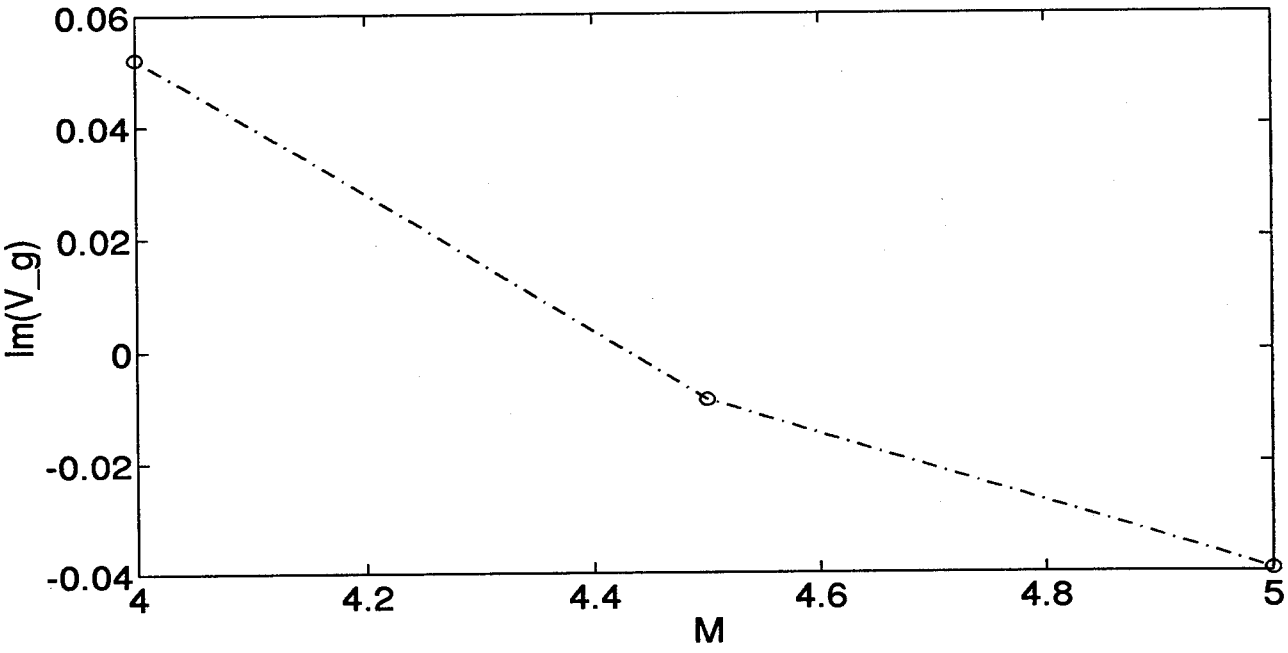
0.06
0.04
0.02
0
-0.02
-0.04
Im(V_g)
4
4.2
4.4
4.6
4.8
5
M

FIGURE 19

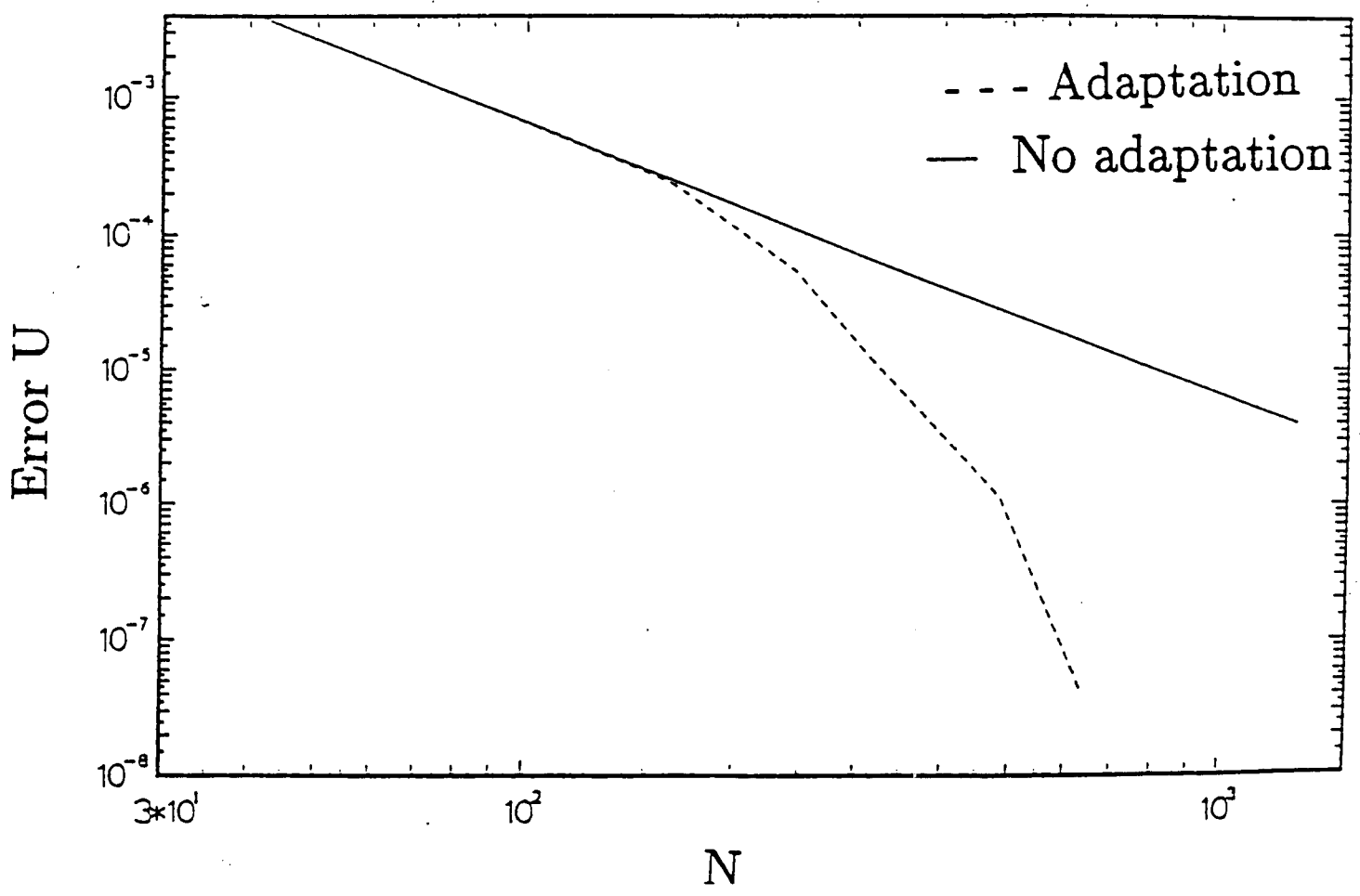
Error U
N
- - - Adaptation
— No adaptation
10^-3
10^-4
10^-5
10^-6
10^-7
10^-8
3*10^1
10^2
10^3

FIGURE 20

References

Akima, H., 1970, A new Method of Interpolation and Smooth Curve Fitting based on Local Procedures. J.A.C.M., **17.4**, 589-602.

Anderson, D. A., Tannehill, J. C. & Pletcher R. H., 1984, *Computational Fluid Mechanics and Heat Transfer,* Hemisphere Publishing.

Anderson, J. D., 1989, *Hypersonics and High Temperature Gas Dynamics,* McGraw-Hill.

Bertolli, F. P., 1991, *Compressible Boundary Layer Stability Analyzed with the PSE Equations,* AIAA 91-1637.

Cebeci, T. & Smith, A. M. O., 1974, *Analysis of turbulent boundary layers,* Academic Press, N. Y.

Chang, C. L. & Malik, M. R., 1991, *Compressible stability of growing boundary layers using the Parabolized Stability Equations,* AIAA 91-1636.

Cohen C. B. & Reshotko, E., 1956, *Similar solutions for the compressible laminar boundary layer with heat transfer and pressure gradient,* NACA Report 1293.

Drazin, P. G. & Reid, W. H., *Hydrodynamic Stability,* Cambridge University Press.

Eiseman, P. R., 1987, Adaptive Grid Generation, *Comp. Meth. Appl. Mech. and Eng.*,**64** 321-376, North–Holland.

Erlebacher, G. & Hussaini, M. Y., 1989, Non-Linear Evolution of a Second Mode Wave in Supersonic Boundary Layers, *ICASE Report 89-15.*.

Erlebacher, G. & Hussaini, M. Y., 1990, Numerical Experiments in Supersonic Boundary-Layer Stability, *Physics of Fluids*, **A2**, 94-104.

Guilyardi, E., Van Der Vegt, J.J.W & Ferziger, J.H., 1991, Linear stability analysis of hypersonic boundary layers, Center for Turbulence Research, *Annual research briefs.*

Hackbusch, W., 1985, *Multi-grid methods and applications*,Springer - Verlag, Berlin.

Iyer, V, & Harris, J.E., 1989, Three-dimensional compressible boundary-layer calculations to fourth-order accuracy on wings and fuselages, *AIAA 89-0130.*

Iyer, V, & Harris, J.E., 1990, Fourth–order accurate three–dimensional compressible boundary–layer calculations, *J. Aircraft*, **27.3**, 253-262.

Jordison, R., 1970a, The flat plate boundary layer. Part 1. Numerical integration of the Orr-Sommerfeld equation, *J. Fluid Mech*, **43.4**, 801-811.

Jordison, R., 1970b, The flat plate boundary layer. Part 2. The effect of increasing thickness on stability, *J. Fluid Mech*, **43.4**, 813-818.

Keller, H. B., 1978, Numerical methods in boundary-layer theory, *Ann. Rev. Fluid Mech*, **10**, 417-433.

Kendall, J. M., 1975, Wind Tunnel Experiments Relating to Supersonic and Hypersonic Boundary-Layer Transition, *AIAA J.*, **13-3**, 290-299.

King, R. A., 1991, Mach 3.5 Boundary-Layer Transition on a Cone at Angle of Attack, *AIAA 91-1804.*

Mack, L. M., 1965, Compuation of the Stability of the Laminar Compressible Boundary Layer, *Meth. Comp. Phys*, **4**, 247-299.

Mack, L. M., 1975, Linear Stability Theory and the Problem of Supersonic Boundary-Layer Transition, *AIAA J.*, **13.3**, 278-289.

Mack, L. M., 1977, Transition Prediction and Linear Stability Theory, *AGARD CP 224.*

Mack, L.M., 1984a, Special Course on Stability and Transition of Laminar Flow, *AGARD report 709.*

Mack, L.M., 1984b, Remarks on disputed numerical results in compressible boundary-layer stability theory, *Phys. Fluids*, **27**(2), 342-347.

Malik, M.R., 1982, Finite–Difference Solution of the Compressible Stability Eigenvalue problem, NASA Contractor report NAS1-16572.

Malik, M.R., 1989, Prediction and control of transition in hypersonic boundary layers, *AIAA J.*, **27.11**, 1487-1493.

Malik, M.R., 1990, Numerical Methods for Hypersonic Boundary Layer Stability, *J. Comp. Phys.*, **86**, 376-413.

Malik, M. R. & Orszag, S. A., 1981, Efficient Computation of the Stability of Three-Dimensional Compressible Boundary Layers, *AIAA 81-1277.*

Malik, M. R., Chuang S. & Hussaini, M. Y., 1982, Accurate numerical solution of compressible linear stability equations, *J. Appl. Math. Phys.*, **33**, 189-201.

Moraes, A. C. M., Flaherty J. E. & Nagamatsu H. T., 1991, A Study of Compressible Laminar Boundary Layers at Mach Numbers 4 to 30, *AIAA 91-0323.*

Nayfeh, A. H., 1989, Stability of compressible boundary layers, NASA Conference Publication 3020, Vol. I, Part 2.

Obremski, H. J., Morkovin, M. V. & Landahl M., 1969, A portfolio of stability characteristics of incompressible boundary layers, AGARDograph 134.

Radespiel, R., Graage, K. & Bordersen, O., 1991, Transition predictions using Reynolds-averaged Navier-Stokes and linear stability analysis methods, *AIAA 91-1641.*

Reed, H. L. & Balakumar P., 1990, Compressible boundary-layer stability theory, *Phys. Fluids*, **A2**, 1341-1349.

Reshotko, E., 1976, Boundary-Layer Stability and Transition, *Annual Review of Fluid Mechanics*, **8**, 311-349.

Schlichting, H., 1979, *Boundary-Layer Theory, 7th Ed.* McGraw-Hill.

Stewartson, K., 1964, *The theory of laminar boundary layer in compressible fluids.* Clarendon Press, Oxford.

Tani, I. , 1977, History of boundary-layer theory, *Ann. Rev. Fluid Mech*, **9**, 87-111.

Thompson, J. F., Warsi, Z. U. A. & Mastin, C. W., 1985, *Numerical Grid Generation.* North-Holland, New York.

Van Der Vegt, J.J.W & Ferziger, J.H., 1990, Methods for direct simulation of transition in hypersonic boundary layers I, Center for Turbulence Research, *Annual research briefs.*

Van Der Vegt, J.J.W & Ferziger, J.H., 1991, Methods for direct simulation of transition in hypersonic boundary layers II, Center for Turbulence Research, *Annual research briefs.*

Van Driest, E.R., 1952, Investigation of laminar boundary layer in compressible fluids using the Crocco method, NACA TN 2597.

Vinokur, M., 1983, On One–Dimensional Stretching Functions for Finite Difference Calculations, *J. Comp. Phys.*, **50**, 215-234.

Wazzan, A. R, Okamura, T. T. & Smith A. M. O., 1968, Spatial and temporal stability charts for the Falkner-Skan boundary-layer profiles, *Douglas Aircraft Company Report No. DAC-67086.*

Wazzan, A. R., 1970, The stability and transition of heated and cooled incompressible laminar boundary layers, 4th. International Heat Transfer Conference 1970, Vol. II, Elsevier Pub. Amsterdam.

Wazzan, A. R., Taghavi, H. & Keltner G., 1984, The effect of Mach number on the spatial stability of adiabatic flat plate flow to oblique disturbances, *Phys. Fluids*, **27**(2), 331-340.

White, F. M., 1991, *Viscous Fluid Flow, 2nd ed.* Mc Graw-Hill.

Wilkinson, J. H., 1965, *The Algebraic Eigenvalue Problem*, Oxford University Press, London.

Wornom, S.F., 1977, A critical study of higher–order numerical methods for solving the boundary–layer equations, AIAA 77-637.

Appendix I

The non-zero coefficients of the 5×5 matrices B and C of Eq. (5.8) are given below.

$$B_{11} = \frac{1}{\mu}\frac{d\mu}{dT}T'$$

$$B_{12} = \mathrm{i}(\lambda - 1)(\alpha^2 + \beta^2)$$

$$B_{14} = \frac{1}{\mu}\frac{d\mu}{dT}(\alpha U' + \beta W')$$

$$B_{21} = \mathrm{i}(\lambda - 1)/\lambda$$

$$B_{22} = \frac{1}{\mu}\frac{d\mu}{dT}T'$$

$$B_{23} = -\frac{R}{\mu\lambda}$$

$$B_{32} = 1$$

$$B_{41} = 2(\gamma - 1)M^2\sigma(\alpha U' + \beta W')/(\alpha^2 + \beta^2)$$

$$B_{44} = \frac{2}{\mu}\frac{d\mu}{dT}T'$$

$$B_{45} = 2(\gamma - 1)M^2\sigma(\alpha W' - \beta U')/(\alpha^2 + \beta^2)$$

$$B_{54} = \frac{1}{\mu}\frac{d\mu}{dT}(\alpha W' - \beta U')$$

$$B_{55} = \frac{1}{\mu}\frac{d\mu}{dT}T'$$

$$C_{11} = -\left[\frac{\mathrm{i}R}{\mu T}(\alpha U + \beta W - \omega) + \lambda(\alpha^2 + \beta^2)\right]$$

$$C_{12} = -\left[\frac{R}{\mu T}(\alpha U' + \beta W') + \mathrm{i}\frac{1}{\mu}\frac{d\mu}{dT}T'(\alpha^2 + \beta^2)\right]$$

$$C_{13} = -\frac{\mathrm{i}R}{\mu}(\alpha^2 + \beta^2)$$

$$C_{14} = (\alpha U' + \beta W')\frac{1}{\mu}\frac{d^2\mu}{dT^2}T' + (\alpha U'' + \beta W'')\frac{1}{\mu}\frac{d\mu}{dT}$$

$$C_{21} = \mathrm{i}\frac{\lambda - 2}{\lambda}\frac{1}{\mu}\frac{d\mu}{dT}T'$$

$$C_{22} = -\left[\frac{\mathrm{i}R}{\mu T\lambda}(\alpha U + \beta W - \omega) + (\alpha^2 + \beta^2)/\lambda\right]$$

$$C_{24} = \frac{\mathrm{i}}{\lambda}\frac{1}{\mu}\frac{d\mu}{dT}(\alpha U' + \beta W')$$

$$C_{31} = \mathrm{i}$$

$$C_{32} = -\frac{T'}{T}$$

$$C_{33} = \mathrm{i}\gamma M^2(\alpha U + \beta W - \omega)$$

$$C_{34} = -\tfrac{\mathrm{i}}{T}(\alpha U + \beta W - \omega)$$

$$C_{42} = -\left[\tfrac{R\sigma}{\mu T}T' - 2\mathrm{i}(\gamma-1)M^2\sigma(\alpha U' + \beta W')\right]$$

$$C_{43} = \tfrac{\mathrm{i}R\sigma}{\mu}(\gamma-1)M^2(\alpha U + \beta W - \omega)$$

$$C_{44} = -\Big[\tfrac{\mathrm{i}R\sigma}{\mu T}(\alpha U + \beta W - \omega) + (\alpha^2+\beta^2)$$
$$-(\gamma-1)\sigma M^2 \tfrac{1}{\mu}\tfrac{d\mu}{dT}(U'^2 + W'^2)$$
$$-\tfrac{1}{\mu}\tfrac{d^2\mu}{dT^2}T'^2 - \tfrac{1}{\mu}\tfrac{d\mu}{dT}T''\Big]$$

$$C_{52} = -\tfrac{R}{\mu T}(\alpha W' - \beta U')$$

$$C_{54} = -\tfrac{1}{\mu}\tfrac{d^2\mu}{dT^2}T'(\alpha W' - \beta U') + \tfrac{1}{\mu}\tfrac{d\mu}{dT}(\alpha W'' - \beta U'')$$

$$C_{55} = -\left[\tfrac{\mathrm{i}R}{\mu T}(\alpha U + \beta W - \omega) + (\alpha^2+\beta^2)\right]$$

The primed quantities are the derivatives with respect to the boundary-layer coordinate y. λ is defined as $2/3(\mu_2 + 2)$ where μ_2 is the ratio of the second coefficient of viscosity to the first.

All the velocities have been scaled by U_e, the streamwise component of velocity at the edge of the boundary layer, and all the lengths have been scaled by δ^*, the displacement thickness. The resulting Reynolds and Mach numbers are then given by

$$R = \tfrac{\rho_e U_e \delta^*}{\mu_e}$$

$$M = \tfrac{U_e}{\sqrt{\gamma \Re T_e}}$$

where ρ_e, μ_e and T_e are the density, viscosity and mean temperature in the free stream.

These coefficients are for the 3D flow. In the code W is set to zero.

Appendix II

The non-zero coefficients a_{ij} of Eq. (5.10) are given below.

$$a_{12} = 1$$

$$a_{21} = \frac{\mathrm{i}\xi\mathrm{R}}{\mu\mathrm{T}} + (\alpha^2 + \beta^2)$$

$$a_{22} = -\frac{1}{\mu}\frac{d\mu}{dT}T'$$

$$a_{23} = \frac{R}{\mu T}(\alpha U' + \beta W') - \mathrm{i}(\alpha^2 + \beta^2)\left[\frac{1}{\mu}\frac{\mathrm{d}\mu}{\mathrm{dT}}\mathrm{T}' + \mathrm{l}_1\frac{\mathrm{T}}{\mathrm{T}'}\right]$$

$$a_{24} = \frac{\mathrm{iR}}{\mu}(\alpha^2 + \beta^2) - (\alpha^2 + \beta^2)l_1\gamma M^2\xi$$

$$a_{25} = -\frac{1}{\mu}\frac{d\mu}{dT}(\alpha U'' + \beta W'') - \frac{1}{\mu}\frac{d^2\mu}{dT^2}T'(\alpha U' + \beta W') + \frac{l_1\xi}{T}(\alpha^2 + \beta^2)$$

$$a_{26} = -\frac{1}{\mu}\frac{d\mu}{dT}(\alpha U' + \beta W')$$

$$a_{31} = -\mathrm{i}$$

$$a_{33} = \frac{T'}{T}$$

$$a_{34} = -\mathrm{i}\gamma\mathrm{M}^2\xi$$

$$a_{35} = \frac{\mathrm{i}\xi}{\mathrm{T}}$$

$$a_{41} = -2\mathrm{i}\chi\frac{1}{\mu}\frac{\mathrm{d}\mu}{\mathrm{dT}}\mathrm{T}' - \mathrm{i}\chi\mathrm{l}_2\frac{\mathrm{T}'}{\mathrm{T}}$$

$$a_{42} = -\mathrm{i}\chi$$

$$a_{43} = -\chi\left[\frac{\mathrm{iR}\xi}{\mu\mathrm{T}} + (\alpha^2 + \beta^2) - l_2\frac{1}{\mu}\frac{d\mu}{dT}\frac{T'^2}{T} - l_2\frac{T''}{T}\right]$$

$$a_{44} = \chi\left[-\mathrm{il}_2\gamma\mathrm{M}^2\xi\left(\frac{1}{\mu}\frac{\mathrm{d}\mu}{\mathrm{dT}}\mathrm{T}' + \frac{\mathrm{T}'}{\mathrm{T}}\right) - \mathrm{il}_2\gamma\mathrm{M}^2(\alpha\mathrm{U}' + \beta\mathrm{W}')\right]$$

$$a_{45} = \chi\left[\mathrm{il}_2\xi\frac{1}{\mu}\frac{\mathrm{d}\mu}{\mathrm{dT}}\frac{\mathrm{T}'}{\mathrm{T}} + \mathrm{i}\left(\frac{1}{\mu}\frac{\mathrm{d}\mu}{\mathrm{dT}} + \frac{\mathrm{l}_2}{\mathrm{T}}\right)(\alpha\mathrm{U}' + \beta\mathrm{W}')\right]$$

$$a_{46} = \frac{\mathrm{i}\chi\mathrm{l}_2\xi}{\mathrm{T}}$$

$$a_{56} = 1$$

$$a_{62} = -2(\gamma - 1)M^2\sigma(\alpha U' + \beta W')/(\alpha^2 + \beta^2)$$

$$a_{63} = \frac{R\sigma}{\mu T}T' - 2\mathrm{i}(\gamma-1)\mathrm{M}^2\sigma(\alpha\mathrm{U}' + \beta\mathrm{W}')$$

$$a_{64} = -\mathrm{i}(\gamma-1)\mathrm{M}^2\frac{\mathrm{R}\sigma}{\mu}\xi$$

$$a_{65} = \frac{\mathrm{iR}\sigma\xi}{\mu\mathrm{T}} + (\alpha^2+\beta^2) - \frac{\mu''}{\mu} - (\gamma-1)M^2\sigma\frac{1}{\mu}\frac{d\mu}{dT}(U'^2 + W'^2)$$

$$a_{66} = -\frac{2}{\mu}\frac{d\mu}{dT}T'$$

$$a_{68} = -2(\gamma-1)M^2\sigma(\alpha W' - \beta U')/(\alpha^2+\beta^2)$$

$$a_{78} = 1$$

$$a_{83} = \frac{R}{\mu T}(\alpha W' - \beta U')$$

$$a_{85} = -\frac{1}{\mu}\frac{d\mu}{dT}(\alpha W'' - \beta U'') - \frac{1}{\mu}\frac{d^2\mu}{dT^2}T'(\alpha W' - \beta U')$$

$$a_{86} = -\frac{1}{\mu}\frac{d\mu}{dT}(\alpha W' - \beta U')$$

$$a_{87} = \frac{\mathrm{iR}\xi}{\mu\mathrm{T}} + (\alpha^2+\beta^2)$$

$$a_{88} = -\frac{1}{\mu}\frac{d\mu}{dT}T'$$

where $(\ ) \equiv d/dy$, $\xi = (\alpha U + \beta W - \omega)$, $\chi = \frac{1}{\frac{R}{\mu}+\mathrm{i}\gamma\mathrm{M}^2\xi\mathrm{l}_2}$ and $l_j = j + \lambda/\mu$.

Acknowledgements

The authors gratefully acknowledge the financial support by AFOSR (Grant F49620-92-J-0005, Technical Monitor: Leonidas Sakell). The authors also thank Drs. Jaap J. Van der Vegt and Chris Hill for fruitful discussions and Dr. M. R. Malik for the original version of the code and San Diego Supercomputer Center (SDSC) for the computer resources. Mr. Eric Guilyardi did much of the exploratory part of the work reported herein.

The code is available on request from the authors.